A SOURCE DISTRIBUTION TECHNIQUE FOR THE SOLUTION OF GENERAL ELECTROMAGNETIC SCATTERING PROBLEMS

PHASE 1 REPORT

13 OCTOBER 1965

Contract Number AF33(615)3166
Air Force Avionics Laboratory
Wright-Patterson Air Force Base, Ohio

NOR-65-271

NORTHROP CORPORATION
NORAIR DIVISION
3901 West Broadway
Hawthorne, California 90250

TABLE OF CONTENTS

SECTION			PAGE
	FOREWORD		iii
	SUMMARY		iv
	ILLUSTRATIONS		v
	TABLES		vii
	SYMBOL DEFINITIONS		viii
	NOTATIONS		x
1.0	INTRODUCTION		1
	1.1	Problem Area	1
	1.2	State of the Art	2
2.0	THE SOURCE DISTRIBUTION TECHNIQUE		4
	2.1	Two-Dimensional Formulation	4
		2.1.1 Derivation of the Integral Equation	4
		2.1.1.1 TM Mode (E_z^{inc}) Propagation	5
		2.1.1.2 TE Mode (H_z^{inc}) Propagation	8
		2.1.2 Scattering Cross-Section	9
		2.1.3 Numerical Solution of the Integral Equation	10
		2.1.4 Application to Two-Dimensional Geometries	11
	2.2	Three-Dimensional Formulation	13
		2.2.1 Derivation of the Integral Equation	13
		2.2.2 Scattering Cross-Section	18
		2.2.3 Numerical Solution of the Integral Equation	19

TABLE OF CONTENTS (Continued)

SECTION		PAGE
	2.2.4 Application to Arbitrary Three-Dimensional Geometries	27
3.0	"PHYSICAL OPTICS" TECHNIQUE	27
	3.1 General Formulation	27
	3.2 Numerical Results	30
4.0	"SDT - PHYSICAL OPTICS" PROCEDURES	31
5.0	IMAGE PLANE REFLECTIVITY RANGE	31
6.0	CONCLUSIONS	33
7.0	REFERENCES	34

FOREWORD

The objective of this program is to develop general procedures for the determination of electromagnetic scattering from arbitrary surfaces with application to optimization of vehicle, antenna, and radome designs.

This document is principally a compilation of the following technical reports and memos issued during the course of this investigation.

1. Technical Data: "Scattering of a Plane Magnetic Wave from a Conducting Circular Cylinder" - Fred Oshiro, 1 February 1963.
2. Technical Data: "Scattering of a Plane Electric Wave from a Conducting Circular Cylinder" - Fred Oshiro, 7 February 1963.
3. Technical Data: "A Source Distribution Technique for the Solution of General Electromagnetic Scattering Problem" - February 1963.
4. NB 63-125: "Proposal for a Source Distribution Technique for the Solution of General Electromagnetic Scattering Problem" - April 1963.
5. Addendum & Technical Data (Item 3) dated 23 May 1964.
6. Preliminary Data, "A Source Distribution Technique for the Solution of General Electromagnetic Scattering Problems", dated 14 May 1964.
7. Addendum to Item (6) dated 14 December 1964.

The technique described herein is being further developed and extended to solve arbitrary geometries under contract AF 33(615)- 3166 .. "Calculation of Radar Cross Section" - Wright Patterson Air Force Base, Ohio.

SUMMARY

A Source Distribution Technique ("SDT") for the solution of general electromagnetic problems has been developed by the Electronic Systems Research Group of Northrop Norair. This technique embodies a comparatively simple and unrestricted computational method applicable to the complex problem of scattering from arbitrarily shaped geometries. The procedure exhibits a greater degree of flexibility and accuracy than present day approximation techniques. It is a numerical procedure for determination of the radar cross section for complex targets, based on an integral equation approach. It can be employed to determine the electromagnetic scattering from arbitrarily shaped two-and-three-dimensional geometries in the difficult resonant frequency ranges in which classical solutions are not available. Combined with the Norair Physical Optics procedure the "SDT" can be employed to determine the electromagnetic scattering of a variety of shapes, including large scattering objects; i.e. $>2\lambda$.

Verification of the technique was performed on the Norair radar reflectivity range. An image-plane was utilized to measure the current distribution and scattered fields. A brief outline of the basic procedure is described together with a few examples to demonstrate its validity.

ILLUSTRATIONS

FIGURE		PAGE
1	Current Distribution on Circular Cylinder, H_z^{inc} (Vert. Pol.) (ka = 1.6)	35
2	Current Distribution on Circular Cylinder, E_z^{inc} (Hor. Pol.) (ka = 1.6)	36
3	Scattering Cross-Section of Circular Cylinder, H_z^{inc} (Vert. Pol.) (ka = 1.6)	37
4	Scattering Cross-Section of Circular Cylinder, E_z^{inc} (Hor. Pol.) (ka = 1.6)	37
5	Current Amplitude Distribution on Elliptic Cylinder, H_z^{inc} (Vert. Pol.)	38
6	Current Phase Distribution on Elliptic Cylinder, H_z^{inc} (Vert. Pol.)	38
7	Scattering Cross-Section of Elliptic Cylinder, H_z^{inc} (Vert. Pol.)	39
8	Airfoil Section #1	40
9	Airfoil Section #2	41
10	Scattering Cross-Section of Airfoil #1 H_z^{inc} (Vert. Pol.)	42
11	Scattering Cross-Section of Airfoil #2 H_z^{inc} (Vert. Pol.)	43
12	Current Distribution on Sphere $F_{\bar{\theta}}(\theta)$ Component, (ka = 1.7)	44
13	Current Distribution on Sphere $F_{\bar{\theta}}(\phi)$ Component, (ka = 1.7)	44

ILLUSTRATIONS (Continued)

FIGURE		PAGE
14	Bistatic Cross-Section of Sphere, (ka = 1.7)	45
15	Bistatic Cross-Section of Spheroid, (ka = 1.7)	46
16	Bistatic Cross-Section of Cone (ka = 1.7)	47
17	Bistatic Cross-Section of Cone-Sphere (ka 1.7)	48
18	Backscattering Cross-Section of Perfectly Conducting Sphere	49
19	Bistatic Cross-Section for Perfectly Conducting Sphere (ka = 10) H-Plane	49
20	Monostatic Cross-Section of Circular Cylinder (R = 1.21λ, L = 2.42λ)	50
21	Monostatic Cross-Section of Circular Cylinder (R = 1.145λ, L = 7.91λ)	51
22	Application of "SDT-P/O" Techniques on Bodies in Transition Region	52
23	"SDT - Physical Optics" Bistatic Cross-Section of Sphere (ka = 4.1)	52
24	Hemi-Surface Mounted on Image-Plane	53
25	Image-Plane With Absorbing Material	53
26	Ground Plane Reflectivity Range	54

LIST OF TABLES

TABLE		PAGE
1	Current Polarities on an Axially Symmetrical Body	24
2	Current Polarities on Bodies with Plane of Symmetry	24
3	Symmetrical Subsurfaces for Axially Symmetric Shapes	25
4	Radar Cross Section (σ) of Some Simple Shapes	55

SYMBOL DEFINITIONS

$\hat{a}$ = arbitrary constant vector

$\hat{E}(r)$ = electric field vector

F = unknown current

$\hat{F}(r)$ = induced current vector

F_t = $C + jD$ = transverse current

F_z = $A + jB$ = longitudinal current

$\hat{G}(r', r)$ = Green's function

$\hat{H}(r)$ = magnetic field vector

$H_o^{(1)}(kr)$ = zero order Hankel function of the first kind

$H_1^{(1)}(kr)$ = first order Hankel function of the first kind

j = unit imaginary number ($j^2 = -1$)

k = $\frac{2\pi}{\lambda}$ = wave number

K = incident field

$\hat{n}$ = unit normal vector = $\ell\hat{x} + m\hat{y} + n\hat{z}$

$\hat{n}_P$ = unit normal at point P = $\ell_P \hat{x} + m_P \hat{y} + n_P \hat{z}$

n = number of surface elements

r = $x^2 + y^2 + z^2$ = observation point in region V

S = surfaces of region V

t = transverse component

NOTATIONS

Subscripts:

P = observation point on scatterer

Q = source point on scatterer

1 = obstacle surface

2 = outer surface

t = transverse component

z = longitudinal component in z direction

Superscripts:

primed variables = represents source points

unprimed variables = represents observation points

in = incident wave

sc = scattered wave

1.0 INTRODUCTION

1.1 Problem Area

Rapidly advancing weapon system technologies have created a renewed interest in the study of scattering and diffraction problems. A current concern is with evaluation and control of radar cross section (RCS). Much effort has been directed at reducing RCS by camouflaging techniques and by use of radar absorbing material (RAM); additional efforts are directed at RCS enhancement of drones and decoy applications for penetration aids. There is an acute interest in reflectivity signature for vehicle identification. Northrop Norair's studies in this field have been motivated by a need to optimize vehicle shapes compatible with both aerodynamic performance and RCS requirements. Solutions to these scattering problems are of vital interest to the design engineer.

The computation of scattering from an arbitrary obstacle is intrinsically complicated, since it depends on several parameters as frequency, polarization, direction of incident wave, observation angle, configuration, and material of the body. The fundamental problem in computation is the explicit determination of the far field parameters of amplitude, phase, and polarization by solution of the basic wave equation.

Traditionally, solutions to the wave equation have been achieved by the separation of variables or eigenfunction expansion, asymptotic evaluation of an integral equation, and the optical approximation techniques. The restrictions imposed by these methods have limited their usefulness in many practical engineering problems. The requirement that the body configuration be completely defined in a coordinate system has led to special mathematical functions that are tabulated for only a few simple shapes. Asymptotic expansions lead to infinite series, whose convergence behaviors are determined by the "electromagnetic size" of the body, therefore, for practical reasons, only

"small" shapes have been examined. In contrast, the "optical" techniques are valid only for "large" shapes.

An immediate dilemma arises when the design engineer is faced with a scattering problem in which the geometrical shape does not "fit" the above requirements. The problem usually is approached by intelligent application of known solutions from simpler shapes, or by relying heavily on reflectivity range data. A need then exists for a general method for evaluating the scattering and diffraction problems encountered in the design of practical electromagnetic systems.

1.2 State of the Art

Since the solution of electromagnetic scattering and diffraction problems is difficult, the introduction of the above restrictions was not without foundation. In order to gain insight as well as attach physical significance to the theoretical studies, it was natural that the classical studies be concentrated on small, simple, and idealized bodies. Most of the present day approximation procedures for complex structures are usually tested against the exact solutions from simpler shapes. The simple body solutions provide the only means for calibrating experimental techniques to measure scattering and diffraction phenomena. Also the knowledge gained by a detailed study of the simpler shapes is used as stepping stones to the study of more complicated shapes.

The accomplishments of Siegel and his group at the University of Michigan together with the Antenna Laboratory Group at Ohio State University, constitute a major contribution in recent years (References 1 and 2). Their procedure was to assume that the various parts of a large complex shape (such as an aircraft) scatter

independently. They approximated the parts by relatively simple shapes, computed the scattering from each shape, and combined the individual contributions to obtain the total scattered field. Their results yield good agreement between theory and experiment. However, for critical aspect angles large errors arise which are generally attributed to the inability of the method to properly model the resonance of the fine structure (i.e., ducts and engine nacelle).

In attempting solutions to more general configurations, the emphasis is usually placed on the desirability of attaining purely analytical solutions. The study of numerical solutions has been neglected but not overlooked. In 1959 Sinclair (Reference 3) emphasizes the need for more general methods of solving boundary-value problems. He also pointed out that there may be certain advantages of numerical solutions in the "resonance region." The usefulness of numerical techniques in the solution of potential flow problems (Laplace's equation) in aerodynamics and hydrodynamics has been demonstrated by Smith (Reference 4) and Hess (Reference 5). In addition to solving general problems involving two-dimensional and axially symmetric bodies, they have provided general techniques for the solution of arbitrary three-dimensional shapes. There is a very limited supply of numerical procedures for general electromagnetic scattering problems.

It is the purpose of this report to describe a method based on the numerical solution of an integral equation which is capable of giving excellent results in this range. Additionally, by application of the principles of physical optics, the technique is extended to include "large" objects and has the unique feature of eliminating much of the guesswork associated with the current customary physical optics procedures.

2.0 THE SOURCE DISTRIBUTION TECHNIQUE ("SDT")

2.1 Two-Dimensional Formulation

2.1.1 Derivation of the Integral Equation

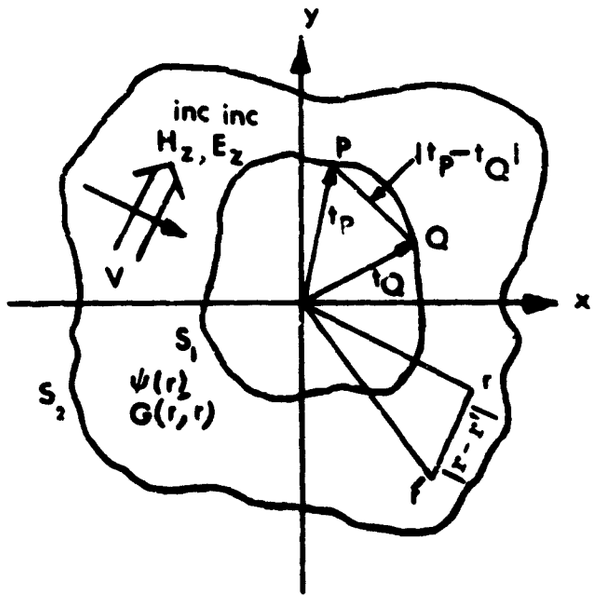

In the volume V enclosed by surfaces, S_1 and S_2 assume there exists two scalar potential functions $\psi(r)$ and G (r', r) such that $\psi(r)$ satisfies the homogeneous wave equation,

$$(\nabla^2 + k^2)\,\psi(r) = 0$$
$$\psi(r) \to 0 \text{ as } r \to \infty \tag{1}$$

and the Green's function G (r', r) satisfies the wave equation.

$$(\nabla^2 + k^2)\,G(r', r) = -\,\delta(r - r'),$$
$$G(r', r) \to 0 \text{ as } r \to \infty. \tag{2}$$

Applying Green's Theorem to $\psi(r)$ and G (r', r) we obtain

$$\int_V \left[G\,(r',\ r)\,(\nabla'^2 + k^2)\,\psi\,(r') - \psi(r')\,(\nabla'^2 + k^2)\,G\,(r',\ r)\right] dv'$$

$$= \int_{S_1 + S_2} \left[G\,(r', r) \frac{\partial}{\partial n'}\,\psi\,(r') - \psi\,(r') \frac{\partial}{\partial n'}\,G\,(r', r) \right] ds' \qquad (3)$$

where the normal derivative on the surface is taken in the direction of the inward normal.

However, in virtue of Equation 1,

$$\int_V \left[G\,(r',\ r)\,(\nabla'^2 + k^2)\,\psi\,(r')\right] dv' = 0\ , \qquad (4)$$

also from the definition of the delta function

$$-\int_V \left[\psi\,(r')\,(\nabla'^2 + k^2)\,G\,(r',\ r)\right] dv' =$$

$$-\int_V \psi\,(r') \left[-\delta\,(r - r')\right] dv' = \psi\,(r)\ . \qquad (5)$$

Equation 3 becomes,

$$\psi\,(r) = \int_{S_2} \left[G\,(r',\ r) \frac{\partial}{\partial n'}\,\psi\,(r') - \psi\,(r') \frac{\partial}{\partial n'}\,G\,(r',\ r)\right] ds'$$

$$+ \int_{S_1} \left[G\,(r',\ r) \frac{\partial}{\partial n'}\,\psi\,(r') - \psi\,(r') \frac{\partial}{\partial n'}\,G\,(r',\ r)\right] ds'\ . \qquad (6)$$

The total field at r, is composed of an incident and scattered field,

$$\psi^{\text{total}}(r) = \psi^{\text{inc}}(r) + \psi^{\text{sc}}(r). \tag{7}$$

It can be shown, (References 6 and 7) that the integral over S_2 reduces to $\psi^{\text{inc}}(r)$ and the integral over S_1 represents the scattered field.

Equation 6 becomes

$$\psi^{\text{total}}(r) = \psi^{\text{inc}}(r) + \int_{S_1} \left[G(r', r) \frac{\partial}{\partial n'} \psi(r') - \psi(r') \frac{\partial}{\partial n'} G(r', r) \right] ds' \tag{8}$$

and represents the integral equation of the field at r in terms of an incident field contribution and a surface integral contribution.

2.1.1.1 TM Mode (E_z^{inc}) Propagation

For the case of TM mode propagation in the two dimensional domain the electric field can be expressed as

$$\hat{E}(r) = \psi(\rho, \phi)\hat{z} = E_z(t)\hat{z} \tag{9}$$

where z is taken as the separation direction and t represents the transverse components. (This propagation mode corresponds to horizontal polarization). Substituting this expression in Equation 8 yields,

$$E_z^{\text{total}}(t) = E_z^{\text{inc}}(t) + \int_{S_1} \left[G(t', t) \frac{\partial}{\partial n'} E_z^{\text{total}}(t') - E_z^{\text{total}}(t') \frac{\partial}{\partial n'} G(t', t) \right] ds' \tag{10}$$

The free space Green's function in the two dimensional domain is the zero order Hankel function of the first kind,

$$G(\rho', \theta'; \rho, \theta) = \frac{i}{4} H_0^{(1)}\left(k\sqrt{\rho^2 + \rho'^2 - 2\rho\rho' \cos(\theta - \theta')}\right) \quad (11)$$

$$\text{or} \qquad G(t', t) = \frac{i}{4} H_0^{(1)}(k|t - t'|) \,. \quad (12)$$

If S_1 is perfectly conducting, the total electric field vanishes on the surface,

$$E_z^{\text{total}}(t) = E_z^{\text{inc}}(t) + E_z^{\text{sc}}(t) = 0 \,. \quad (13)$$

Therefore when the observation point is taken on the surface, Equation 10 reduces to

$$0 = E_z^{\text{inc}}(t) + \frac{i}{4} \int_{S_1} H_0^{(1)}(k|t - t'|) \cdot \frac{\partial}{\partial n'} E_z^{\text{total}}(t')\, ds' \,. \quad (14)$$

The quantity $\frac{\partial}{\partial n'} E_z^{\text{total}}(t')$ is the unknown current induced on S_1 by the incident electric field. The direction of current flow is in the direction of the electric field, e.g., the z direction. Setting,

$$\hat{F}_z(t') = \frac{\partial}{\partial n'} E_z^{\text{total}}(t')\, \hat{z} \quad (15)$$

and introducing subscripts P and Q for the observation and source points respectively on the surface of the scatterer, we obtain the desired integral equation for the unknown current $F_z(t_Q)$,

$$0 = E_z^{\text{inc}}(t_P) + \frac{i}{4} \int_{S_1} \left[H_0^{(1)}(k|t_P - t_Q|)\; F_z(t_Q) \right] ds_Q \,. \quad (16)$$

2.1.1.2 TE Mode (H_z^{inc}) Propagation

For the case of TE mode propagation, the magnetic field vector may be expressed as follows:

$$\hat{H}(r) = \psi(\rho, \theta)\,\hat{z} = H_z(t)\,\hat{z} \tag{17}$$

where, again, z is taken as the separation direction. (This mode of propagation also corresponds to vertical polarization).

Substituting this expression in Equation 8 yields,

$$H_z^{total}(t) = H_z^{inc}(t) + \int_{S_1} \Big| G(t', t) \frac{\partial}{\partial n'} H_z^{total}(t') - H_z^{total}(t') \frac{\partial}{\partial n'} G(t', t) \Big| ds' . \tag{18}$$

The boundary condition on S_1 for the TE case is

$$\frac{\partial H^{total}}{\partial n'}(t') = 0 . \tag{19}$$

If the observation point is taken on S_1, then Maue (Reference 8) has shown that the induced current at the point of incidence is the average value of the magnetic field at that point, consequently

$$\frac{H_z(t)}{2} = H_z^{inc}(t) - \frac{j}{4} \int_{S_1} H_z^{total}(t') \frac{\partial}{\partial n'} H_0^{(1)}(k|t - t'|)\, ds' . \tag{20}$$

The quantity $H_z^{total}(t')$ is the equivalent unknown current induced on S_1 by the incident magnetic field and flows transverse to the z direction.

$$\hat{F}_t(t') = H_z^{total}(t')\,\hat{t} . \tag{21}$$

The integral equation is,

$$\frac{H_z^{\text{total}}(t_P)}{2} = H_z^{\text{inc}}(t_P)$$

$$+\frac{jk}{4}\int_{S_1}\left[H_1^{(1)}(k|t_P - t_Q|)\cdot F_t(t_Q)\cdot\cos\left(\hat{n},\ (\widehat{t_P - t_Q})\right)\right]ds_Q \quad (22)$$

2.1.2 Scattering Cross-Section

The scattered fields may be evaluated from the current distribution by application of Kirchoff's integral

$$\psi^{sc}(r) = -\int_S \nabla' G(r', r)\times\hat{F}(r')\,ds' \quad (23)$$

Since the observation distance is usually taken to be very large, the asymptotic forms of the Hankel functions may be introduced for the Green's function to give:

$$H_z^{sc}(r) = \left(\frac{2}{\pi kr}\right)^{1/2} e^{j(kr - \pi/4)}\int_S F_t e^{jkr'\cos(\theta - \theta')}\cos(\hat{n}, \hat{r}')\,ds' \quad (24)$$

$$E_z^{sc}(r) = -j\omega\mu\left(\frac{2}{\pi kr}\right)^{1/2} e^{j(kr - \pi/4)}\int_S F_z e^{jkr'\cos(\theta - \theta')}ds' \quad (25)$$

The radar cross section of two-dimensional cylinders is defined as the power scattered per unit axial length to the incident power and has dimensions of length. Thus,

$$\sigma^{sc} = 2\pi r\,\frac{\left|E_z^{sc}(r)\right|^2}{\left|E_z^{inc}(r)\right|^2} = \frac{2\pi r\left|H_z^{sc}(r)\right|^2}{\left|H_z^{inc}(r)\right|^2} \quad (26)$$

where the expressions $E_z^{sc}(r)$ and $H_z^{sc}(r)$ are the scattered fields from Equations 24 and 25 respectively and the integration is taken over the closed contour of the

scatterer. For simplicity the scattering cross-section has been normalized to unity incident power.

2.1.3 Numerical Solution of the Integral Equation

The use of an integral equation to formulate a scattering problem is well known and has been the basis of many approximation techniques. (References 8-14). The present technique differs from classical treatments in that numerical methods are exploited to obtain direct solution for the unknown quantities rather than formal indirect methods. The solution of Equations 16 and 22, for example, may be achieved by first approximating the contour S_1 by n straight line segments and then setting the current distribution constant over each interval.

$$F_{zi} = A_i + j\,B_i \tag{27}$$

$$F_{ti} = C_i + j\,D_i \tag{28}$$

This assumption is valid only if the line segment is less than .12λ. Inserting this expression in Equations 16 and 22 respectively yields

$$-E_z^{inc}(t_p) = \sum_{i=1}^{n} \left| \frac{\left[A_i(t_Q) + j\,B_i(t_Q)\right]}{4} \cdot \int_S H_o^{(1)}\left(k\left|t_p - t_Q\right|\right) ds_Q \right| \tag{29}$$

$$-H_z^{inc}(t_p) = \sum_{i=1}^{n} \left| \frac{C_i(t_Q) + j\,D_i(t_Q)}{2} \right. \tag{30}$$

$$\left. + \frac{jk}{4} \left[C_i(t_Q) + j\,D_i(t_Q)\right] \int_S H_1^{(1)}\left(k\left|t_p - t_Q\right|\right) \cdot \cos\left(\hat{n},\ \widehat{(t_p - t_Q)}\right) ds_Q \right|$$

The integration of the Hankel function is carried out numerically via Simpson's rule. The integral equation is now recast into a set of finite difference equations, wherein the complex coefficients of the unknown currents form an n x n matrix, n being the number of sub-surfaces describing the body. The excitation function is the impinging wave. The unknown currents are determined by solving a matrix equation of the type

$$\left[T\right] \left[F\right] = \left[K\right] \tag{31}$$

where

$\left[F\right]$ = unknown currents

$\left[T\right]$ = Kernel of the integral equation

$\left[K\right]$ = incident field .

Applications of matrix inversion techniques lead to a direct solution of the currents.

2.1.4 Application to Two-Dimensional Geometries

To demonstrate the validity of this technique a classical problem is examined, i.e., scattering from an infinite circular cylinder. The problem is specialized for normal incidence of either a vertically or horizontally polarized wave, resulting in either transverse or longitudinal type currents respectively. These simplifications were introduced to provide suitable comparisons with available classical results. Figures 1 and 2 are comparisons of the current amplitude and phase with the classical series expansion results. (Reference 15). In both examples the diameter of the cylinder was chosen to be $\lambda/2$; and twelve points were distributed equidistant around the periphery to carry out the numerical integration.

The bistatic scattering cross-sections of the circular cylinder for vertical and horizontal polarization are shown in Figures 3 and 4 respectively. The transmitter is fixed at the 180 degree position and the radar cross section is observed at various bistatic angles The quantity characteristics of energy scattered back toward the source is commonly known as the monostatic cross section of the obstacle wherein the transmitter and receiver are both located at the same point. The forward or total scattering cross-section is the value at 0 degrees. Where possible theoretical results have been introduced for suitable comparison with the "SDT" data. Normalization of the results is accomplished by multiplying the cross-section by the wave number, k. (The designation "SDT" in quotation is used to distinguish this technique from other procedures developed during the course of this study).

The flexibility of the "SDT" for the solution of non-circular geometries will be demonstrated. Earlier contributions to generalize the circular cylindrical scattering problems to non-circular shapes were made by Fock (Reference 16). His "universal function" enabled him to determine the surface currents in the penumbra region near to and including the shadow boundary. More recently, Wetzel (Reference 17) following the lead of Fock derived a new set of functions to obtain the currents in the deep shadow region where Fock's approximation was not adequate. Wetzel applied his functions for the solution of the current distribution on a perfectly conducting elliptic cylinder and confirmed his theory with measured data. The "SDT" was applied to the same geometry for comparison. As shown in Figures 5 and 6 the "SDT" shows still greater correlation with the measured data, especially in the deep shadow region. Its bistatic scattering cross-section is shown in Figure 7. The sharp peak in the forward direction is characteristic of large scatterers.

Next, the scattering cross-section of two different airfoil sections shown in Figures 8 and 9 were considered. An incident magnetic plane wave propagating along

the x-axis impinges on the surface of the perfectly conducting two dimensional geometries. Classical results to these geometries have not been possible because of the complexity of solutions. The airfoil shape was approximated by 49 straight line segments distributed along the periphery and the "SDT" was applied. The bi-static cross-sections are shown in Figures 10 and 11.

Several important conclusions concerning the behavior of these scatterers can be made which otherwise would be difficult if not impossible to predict by approximation techniques or by intuition.

1. A large back lobe is developed at 150 degrees in the direction of the trailing edge.
2. Although airfoil section No. 2 is smaller than No. 1, its major back lobe is larger.
3. The monostatic cross sections (at 180°) of the airfoil sections are approximately equal.

2.2 Three Dimensional Formulation

2.2.1 Derivation of the Integral Equation

Aside for the additional complexity of vector fields, the derivation of the integral equation is similar to the two dimensional case.

In the volume V enclosed by surfaces S_1 and S_2 assume there exists two vector fields $\hat{H}(r)$ and $\hat{G}(r', r)$ such that $\hat{H}(r)$ satisfies the homogeneous vector wave equation

$$\nabla \times \nabla \times \hat{H}(r) - k^2 \hat{H}(r) = 0$$

$$\hat{H}(r) \longrightarrow 0 \text{ as } r \longrightarrow \infty \qquad (32)$$

$\hat{H}(r)$ = Magnetic Field

$\hat{G}(r', r) = \varphi(r', r)\,\hat{a}$

$$\varphi(r', r) = \frac{e^{jk|r-r'|}}{4\pi|r-r'|}$$

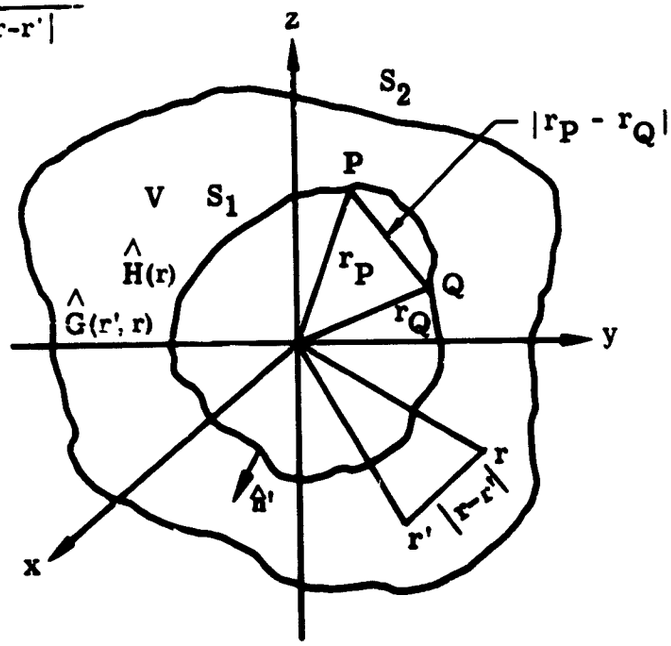

and the vector Green's function $\hat{G}(r', r)$ satisfies the inhomogeneous wave equation

$$\nabla \times \nabla \times \hat{G}(r', r) - k^2 \hat{G}(r', r) = -\delta(r - r')\,\hat{a}$$

$$\hat{G}(r', r) \longrightarrow 0 \text{ as } r \longrightarrow \infty \tag{33}$$

Applying Green's theorem to the wave equation we find

$$\int_V \left\{ \hat{G}(r', r) \cdot \left[\nabla' \times \nabla' \times + k^2 \right] \hat{H}(r') - \hat{H}(r') \cdot \left[\nabla' \times \nabla' \times + k^2 \right] \hat{G}(r', r) \right\} dv'$$

$$= \int_{S_1 + S_2} \left[\hat{H}(r') \times \nabla' \times \hat{G}(r', r) - \hat{G}(r', r) \times \nabla' \times \hat{H}(r') \right] \cdot \hat{n}'\, ds' \tag{34}$$

where the normal $\hat{n}'$ is directed inward toward the volume V.

The left hand side of Equation 34 reduces to

$$- \int_V \hat{H}(r') \cdot \left[- \delta (r - r') \hat{a} \right] d v' = \hat{H}(r) \cdot \hat{a} \quad (35)$$

The vector $\hat{a}$ is assumed constant and arbitrarily oriented within volume V.

Equation 34 becomes,

$$\hat{H}(r) \cdot \hat{a} = \int_{S_2} \left\{ \left[\hat{n} \times \nabla' \times \hat{H}(r') \right] \cdot \hat{G}(r', r) + \hat{n} \times \hat{H}(r') \cdot \left[\nabla' \times \hat{G}(r', r) \right] \right\} d s'$$

$$- \int_{S_1} \left\{ \left[\hat{n} \times \nabla' \times \hat{H}(r') \right] \cdot \hat{G}(r', r) + \hat{n} \times \hat{H}(r') \cdot \left[\nabla' \times \hat{G}(r', r) \right] \right\} d s' \quad (36)$$

Substituting $\hat{H}(r) = \hat{H}^{inc}(r) - \hat{H}^{sc}(r)$ into the first integral of Equation 36 we find

$$\int_{S_2} = - \int_{S_2} \left\{ \hat{n} \times \left[\nabla' \times \hat{H}^{inc}(r') \right] \cdot \hat{G}(r', r) \right.$$

$$\left. + \left[\hat{n} \times \hat{H}^{inc}(r') \right] \cdot \left[\nabla' \times \hat{G}(r', r) \right] \right\} d s' \quad (37)$$

$$- \int_{S_2} \left\{ \hat{n} \times \left[\nabla' \times \hat{H}^{sc}(r') \right] \cdot \hat{G}(r', r) + \left[\hat{n} \times \hat{H}^{sc}(r') \right] \cdot \left[\nabla' \times \hat{G}(r', r) \right] \right\} d s'$$

Applying Green's theorem in reverse to the first integral

$$- \int_{S_2} \left\{ \hat{n} \times \left[\nabla' \times \hat{H}^{inc}(r') \right] \cdot \hat{G}(r', r) + \left[\hat{n} \times \hat{H}^{inc}(r') \right] \cdot \left[\nabla' \times \hat{G}(r', r) \right] \right\} d s$$

$$= \int_V \left[\hat{G}(r', r) \cdot (\nabla' \times \nabla' \times + k^2) \hat{H}^{inc}(r') \right.$$

$$\left. - \hat{H}^{inc}(r') \cdot (\nabla' \times \nabla' \times + k^2) \hat{G}(r', r) \right] d v' \quad (38)$$

$$= - \int_V \hat{H}^{inc}(r') \left[- \delta (r - r') \hat{a} \right] d v' = \hat{H}^{inc}(r) \cdot \hat{a} \qquad (38) \text{ Continued}$$

The second integral vanishes identically since $\hat{H}^{sc}(r')$ and $\hat{G}(r', r)$ both satisfy the radiation condition. Therefore, Equation 36 reduces to

$$\hat{H}(r) \cdot \hat{a} = \hat{H}^{inc}(r) \cdot \hat{a} - \int_{S_1} \left\{ \left[\hat{n} \times \nabla' \times \hat{H}(r') \right] \cdot \hat{G}(r', r) + \hat{n} \times \hat{H}(r') \cdot \left[\nabla' \times \hat{G}(r', r) \right] \right\} d s' \qquad (39)$$

And from Maxwell's equation,

$$\nabla \times \hat{H}(r') = j \omega \epsilon \hat{E}(r') \qquad (40)$$

we find

$$\hat{H}(r) \cdot \hat{a} = \hat{H}^{inc}(r) \cdot \hat{a} - \int_{S_1} \left\{ j \omega \epsilon \left[\hat{n} \times \hat{E}(r') \right] \cdot \hat{G}(r', r) + \left[\hat{n} \times \hat{H}(r') \right] \cdot \left[\nabla' \times \hat{G}(r', r) \right] \right\} d s' \qquad (41)$$

If obstacle S_1 is assumed perfectly conducting then the tangential component of the electric field vanishes, $\hat{n} \times \hat{E}(r') = 0$ and additionally the current induced on S_1 is given by $\hat{n} \times \hat{H}(r') = \hat{F}(r')$.

Equation 41 may be rewritten as

$$\hat{H}(r_P) \cdot \hat{a} = \hat{H}^{inc}(r_P) \cdot \hat{a} - \int_{S_1} \hat{F}(r_Q) \cdot \left[\nabla_Q \times \hat{G}(r_Q, r_P)\right] ds_Q. \quad (42)$$

But,

$$\nabla_Q \times \hat{G}(r_Q, r_P) = \nabla_Q \times \varphi(r_Q, r_P)\,\hat{a} = \varphi(\nabla_Q \times \hat{a})$$

$$+ \nabla_Q \varphi(r_Q, r_P) \times \hat{a} = \nabla_Q \varphi(r_Q, r_P) \times \hat{a} \qquad \text{since } \hat{a} \text{ is a constant vector.}$$

Hence,

$$\hat{H}(r_P) \cdot \hat{a} = \hat{H}^{inc}(r_P) \cdot \hat{a} - \hat{a} \cdot \int_{S_1} \left\{ \nabla_Q \varphi(r_Q, r_P) \times \hat{F}(r_Q) \right\} ds_Q. \quad (43)$$

If the observation point is taken on the surface we obtain the desired integral equation

$$-\frac{\hat{F}(r_P)}{2} = +\hat{H}^{inc}(r_P) \times \hat{n}_P - \int_{S_1} \left[\nabla_Q \varphi(r_Q, r_P) \times \hat{F}(r_Q) \times \hat{n}_P\right] ds_Q. \quad (44)$$

Where subscripts P and Q designate points on the surface of the scatterer and

$$\varphi(r_Q, r_P) = \frac{e^{+jk|r_P - r_Q|}}{4\pi |r_P - r_Q|}$$

$\hat{F}(r_P)$ = current at point P

$\nabla_Q \varphi(r_Q, r_P)$ = gradient of φ with respect to point Q

$$= \sum \frac{\omega_{iP} - \omega_{iQ}}{(r_P - r_Q)^2} \left[1 + jk|r_P - r_Q|\right] \varphi(r_Q, r_P)\ \hat{\omega}_i; \qquad \omega_i = x, y, z.$$

$\hat{H}^{inc}(r_P)$ = incident plane wave at point P

$\hat{n}_P$ = unit normal at point P

$= \ell_P \hat{x} + m_P \hat{y} + n_P \hat{z}$

$|r_P - r_Q| = \sqrt{(x_P - x_Q)^2 + (y_P - y_Q)^2 + (z_P - z_Q)^2}$

S_1 = total surface of the scatterer

ds_Q = element surface at point Q .

2.2.2 Scattering Cross-Section

The scattered field may be obtained by substituting the current distribution in Kirchoff's integral,

$$\hat{H}^{sc}(r) = -\int_S \left[\nabla' \hat{G}(r', r) \times \hat{F}(r')\right] ds' \tag{45}$$

$$= -\int_S \left[\frac{e^{+j\hat{k}\cdot|r - r'|}}{4\pi |r - r'|}\left(\frac{1}{r} + jk\right) \times \hat{F}(r')\right] ds'$$

and for $r >> r'$

$$\hat{H}^{sc}(r) \approx \left|-\frac{jk}{4\pi r}\right| \int_S \left[e^{jk\cdot|r - r'|} \times \hat{F}(r')\right] ds' . \tag{46}$$

The scattering cross-section has the dimension of length^2. Thus

$$\sigma^{sc} = 4\pi r^2 \frac{|\hat{H}^{sc}(r)|^2}{|H_z^{inc}(r)|^2} \tag{47}$$

where $\hat{H}^{sc}(r)$ is given by Equation 46 and the integration is carried out over the entire surface of the scatterer.

2.2.3 Numerical Solution of the Integral Equation

The integral Equation 44 represents the complete formulation of the boundary-value problem with the following boundary conditions:

$$\hat{E}(r) \times \hat{n} = 0 , \quad \hat{H}(r) \times \hat{n}_p = - \hat{F}(r)_.$$

To completely evaluate the unknown currents, the integral equation must be solved for the individual components of $\hat{F}(r)$. For the spherical geometry, the surface may be parameterized in terms of local coordinates $\bar{\theta}$ and $\bar{\omega}$. In this special case there are two components of the unknown current and the governing set of equations are:

$$F_{\bar{\theta}} = 2 \sin \bar{\phi} \, e^{jka \cos \bar{\theta}} + \frac{a^3}{2\pi} \int_0^{\pi} d\bar{\theta} \int_{-\pi}^{\pi} d\bar{\varphi} \, \frac{e^{jkr}}{r^3} (1 + jkr)$$

$$\left\{ \left[\sin \bar{\theta} \sin \bar{\theta} + \cos \bar{\theta} \cos \bar{\theta} \cos (\bar{\varphi} - \bar{\phi}) - \cos (\bar{\varphi} - \bar{\phi}) \right] F_{\bar{\theta}} \right. \tag{48}$$

$$\left. + \left[\sin (\bar{\varphi} - \bar{\phi}) (\cos \bar{\theta} - \cos \bar{\theta}) \right] \right\} F_{\bar{\varphi}}$$

$$F_{\bar{\varphi}} = 2 \cos \bar{\theta} \cos \bar{\phi} \, e^{jka \cos \bar{\theta}} \tag{49}$$

$$- \frac{a^3}{2\pi} \int_{\hat{G}}^{\pi} d\bar{\theta} \int_{-\pi}^{\pi} d\bar{\varphi} \, \frac{e^{jkr}}{r^3} (1 + jkr) \left\{ \left[\; \right] F_{\bar{\varphi}} + \left[\; \right] F_{\bar{\theta}} \right\}_.$$

The coupled set of matrix equations are

$$\left[H_{\bar{\theta}}^{inc}\right] = \left[A\right]\left[F_{\bar{\theta}}\right] + \left[B\right]\left[F_{\bar{\varphi}}\right] \tag{50}$$

$$\left[H_{\bar{\varphi}}^{inc}\right] = -\left[B\right]\left[F_{\bar{\theta}}\right] - \left[A\right]\left[F_{\bar{\varphi}}\right]. \tag{51}$$

By direct extension of the two-dimensional case, the surface was approximated by n elemental areas each having constant surface current density to develop a set of finite difference equations. However, since $\hat{F}(r)$ is composed of two orthogonal components on each surface, the matrix equation will be of order 2n. The technique was applied to the problem of electromagnetic scattering from a sphere due to an incident magnetic field. The diameter of the sphere was chosen to be .541 λ (ka = 1.7) and 72 elemental areas described the complete surface. Because of basic symmetries in the problem the size of the matrix was reduced from 144 x 144 to 36 x 36. A more complete description of symmetry conditions will be given in subsequent paragraphs.

Figures 12 and 13 are comparisons of the $F_{\bar{\theta}}(\bar{\varphi})$ and $F_{\bar{\theta}}(\bar{\phi})$ data (taken about the principal plane) with the classical solutions of King and Wu (Reference 15).

The scattered fields are obtained from the following equations:

$$H_{\theta} = -\frac{1}{4\pi}\int ds_Q \frac{\partial}{\partial r}\left(\frac{e^{jkr}}{r}\right)\left\{\left[\cos\bar{\theta}\,\sin(\bar{\varphi}-\phi)\,F_{\bar{\theta}} + \cos(\bar{\varphi}-\phi)\,F_{\bar{\varphi}}\right]\right\} \tag{52}$$

$$H_{\varphi} = \frac{1}{4\pi}\int ds_Q \frac{\partial}{\partial r}\left(\frac{e^{jkr}}{r}\right)\left\{\left[\sin\bar{\theta}\,\sin\bar{\theta} + \cos\bar{\theta}\cos\bar{\theta}\cos(\bar{\varphi}-\phi)\right]F_{\bar{\theta}} - \sin(\bar{\varphi}-\phi)\cos\bar{\theta}\,F_{\bar{\varphi}}\right\}. \tag{53}$$

The scattering cross-sections are obtained from:

$$\sigma^{sc} = 4\pi r^2 \frac{\int |H_\theta|^2}{|H^{inc}|^2} ds \qquad \text{or} \qquad \sigma^{sc} = 4\pi r^2 \frac{\int |H_\varphi|^2 ds}{|H^{inc}|^2} \tag{54}$$

Comparison of the bistatic cross-section between the "SDT" and classical results are shown in Figure 14.

For more complex geometries it is convenient to expand Equation 8 in the Cartesian coordinate system. Carrying out the indicated operation and resolving the integral equation into separate components we obtain,

$$2\,(H_{oy}\, n_P - H_{oz}\, m_P) =$$

$$- F_x(P) + \frac{1}{2\pi} \int_S \left| T_{xx}\, F_x(Q) + T_{xy}\, F_y(Q) + T_{xz}\, F_z(Q) \right| ds_Q$$

$$2\,(H_{oz}\, \ell_P - H_{ox}\, n_P) = - F_y(P) + \frac{1}{2\pi} \int_S \left| T_{yx}\, F_x(Q) \right. \tag{55}$$

$$\left. + T_{yy}\, F_y(Q) + T_{yz}\, F_z(Q) \right| ds_Q$$

$$2\,(H_{ox}\, m_P - H_{oy}\, \ell_P) = - F_z(P) + \frac{1}{2\pi} \int_S \left| T_{zx}\, F_x(Q) + T_{zy}\, F_y(Q) + T_{zz}\, F_z(Q) \right| ds_Q$$

where

$$\hat{H}_o(P) = H_{ox}\, \hat{x} + H_{oy}\, \hat{y} + H_{oz}\, \hat{z}$$

$$T_{xx} = R(P, Q) \left| (z_P - z_Q)\, n_P + (y_P - y_Q)\, m_P \right|$$

$$T_{xy} = - R\,(P,Q)\,(x_P - x_Q)\,m_P$$

$$T_{xz} = - R\,(P,Q)\,(x_P - x_Q)\,n_P$$

$$T_{y.} = - R\,(P,Q)\,(y_P - y_Q)\,\ell_P$$

$$T_{yy} = R\,(P,Q)\left|(x_P - x_Q)\,\ell_P + (z_P - z_Q)\,n_P\right|$$

$$T_{yz} = - R\,(P,Q)\,(y_P - y_Q)\,n_P$$

$$T_{zx} = - R\,(P,Q)\,(z_P - z_Q)\,\ell_P$$

$$T_{zy} = - R\,(P,Q)\,(z_P - z_Q)\,m_P$$

$$T_{zz} = R\,(P,Q)\left|(x_P - x_Q)\,\ell_P + (y_P - y_Q)\,m_P\right|$$

and

$$R\,(P,Q) = (1 + jk\,|r_P - r_Q|)\,\frac{e^{+jk\,|r_P - r_Q|}}{|r_P - r_Q|^3}$$

If the total surface is approximated by n subsurfaces and we let ΔS_Q denote the subsurface at point Q, the integral of Equation 55 can be replaced by a summation preparatory to numerical integration.

$$2\,(H_{oy}\,n_P - H_{oz}\,m_P) = - F_x\,(P) + \frac{1}{2\pi}\sum_{Q=1}^{n}\left|T_{xx}\,F_x\,(Q)\right.$$

$$\left. + T_{xy}\,F_y\,(Q) + T_{xz}\,F_z\,(Q)\right|\Delta S_Q \qquad (56)$$

$$2\,(H_{oz}\,\ell_P - H_{ox}\,n_P) = -\,F_y\,(P) + \frac{1}{2\pi}\sum_{Q=1}^{n}\Big[T_{yx}\,F_x(Q)$$

$$+\,T_{yy}\,F_y\,(Q) + T_{yz}\,F_z\,(Q)\Big]\,\Delta S_Q \qquad (56)\ \text{continued}$$

$$2\,(H_{ox}\,m_P - H_{oy}\,\ell_P) = -\,F_z\,(P) + \frac{1}{2\pi}\sum_{Q=1}^{n}\Big[T_{zx}\,F_x\,(Q)$$

$$+\,T_{zy}\,F_y\,(Q) + T_{zz}\,F_z\,(Q)\Big]\,\Delta S_Q$$

It should be noted that the summation applies to all n surfaces except for P = Q which is the singularity term represented by the single term outside the summation on the right hand side. The left hand side represents the incident wave, $\hat{H}^{inc}\,(P)$.

Each equation in 56 represents n equations, (P = 1 to n) and the 3n simultaneous linear equations yield solutions of F_x, F_y and F_z on each subsurface.

Equation 56 in matrix form is,

$$\left[T\right]\left[F\right] = \left[K\right] \qquad (57)$$

where

$\left[K\right]$ = incident field $= 2\hat{H}^{inc}\,(P) \times \hat{n}_P$

$\left[F\right]$ = unknown currents

$\left[T\right]$ = Kernel of the integral equation (coefficients of F_x, F_y and F_z in Equation 56)

$[F]$ is readily obtained by multiplying Equation 57 through by the inverse of the coefficient matrix, $[T]^{-1}$,

$$\left|F\right| = \left|T\right|^{-1}\left|K\right| \tag{58}$$

Because of the limited storage capacity of computers maximum accuracy is
ta ined by utilizing the symmetry properties of the scatterer. For the case of
ially symmetric bodies the number of subsurfaces can almost be quadrupled
th the same computer storage. When such properties exist it is possible to combine
the coefficients of the symmetrical terms and thereby reduce the number of un-
owns. Care should be taken to determine the proper direction of the currents hence
signs of the coefficients before combining. For the case of incident plane wave
veling along the z-axis and H polarized in the y direction, the polarities of current
mponents on an axially symmetric body are given in Table 1 with the first quadrant
reference and the other quadrants given in the conventional x-y plane of the right
nded Cartesian coordinates

Table 1 Current Polarities on an Axially Symmetrical Body

Quadrant	F_x	F_y	F_z
I	+	+	+
II	+	-	-
III	+	+	-
IV	+	-	+

For the case of plane symmetry the number of subsurfaces could be doubled
applying the above procedures. With quadrants I and IV as reference, and y-z
plane of symmetry, the polarities of the current components are given in Table 2.

Table 2 Current Polarities on Bodies with Plane of Symmetry

Quadrant	F_x	F_y	F_z
I & IV	+	+	+
II & III	+	-	-

As an example a spheroid of 12 x 12 subsurfaces will be considered

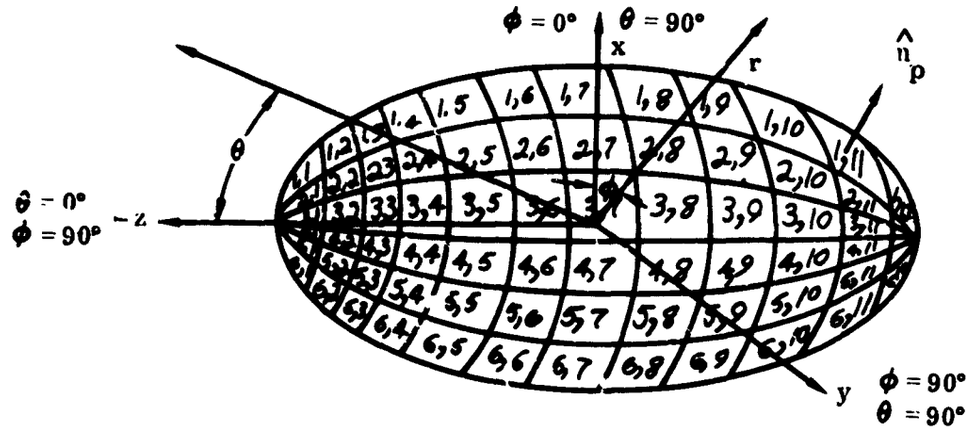

Sketch 1 Spheriod with 12 x 12 Subsurfaces

In Sketch 1 the total surface is divided into twelve sections in both θ and ϕ directions and a set of indices (J, K) is assigned to each subsurface. The first number denotes the order in the θ direction and the second number, the ϕ direction. Table 3 lists the symmetrical subsurfaces whose coefficients are combined to reduce the computer storage.

Table 3 Symmetrical Subsurfaces for Axially Symmetric Shapes

Quadrant	Symmetrical Subsurfaces (K = 1 to 12)		
I	(1, K)	(2, K)	(3, K)
II	(6, K)	(5, K)	(4, K)
III	(7, K)	(8, K)	(9, K)
IV	(12, K)	(11, K)	(10, K)

Once the current on the surface of a scatterer is determined, the far-field pattern can be obtained by applying Kirchoff's integral. Let $\hat{E}_x$, $\hat{E}_y$ and $\hat{E}_z$ denote the three orthogonal components of the electric field at point R (ϑ, ϕ), we have

$$\hat{E}_x = C \sum_{Q=1}^{n} \hat{F}_x(Q)\, e^{j(k_x x_Q + k_y y_Q + k_z z_Q)} \Delta S_Q$$

$$\hat{E}_y = C \sum_{Q=1}^{n} \hat{F}_y(Q)\, e^{j(k_x x_Q + k_y y_Q + k_z z_Q)} \Delta S_Q \qquad (59)$$

$$\hat{E}_z = C \sum_{Q=1}^{n} \hat{F}_z(Q)\, e^{j(k_x x_Q + k_y y_Q + k_z z_Q)} \Delta S_Q$$

where (x_Q, y_Q, z_Q) = coordinates of the current points

$$k_x = k \sin\theta \cos\phi$$

$$k_y = k \sin\theta \sin\phi$$

$$k_z = k \cos\theta$$

C = normalization constant.

Transforming into spherical coordinates, we obtain

$$\hat{E}_\theta = \hat{E}_x \cos\theta \cos\phi + \hat{E}_y \cos\theta \sin\phi - \hat{E}_z \sin\theta$$

$$\hat{E}_\phi = -\hat{E}_x \sin\phi + \hat{E}_y \cos\phi \qquad (60)$$

E_θ and E_ϕ as well as E_x, E_y and E_z are complex quantities and are expressed in terms of real and imaginary components. When the magnitude and the phase are desired it is only a matter of simple conversion, e.g.

$$\left|\hat{E}\right| = \sqrt{E_R^2 + E_I^2}$$

$$\angle\hat{E} = \tan^{-1}\frac{E_I}{E_R} \qquad (61)$$

where

$$\hat{E} = E_R + j\, E_I$$

The scattering cross section at r is then given by

$$\sigma^{sc} = 4\pi r^2 \frac{\left| \left| \hat{E}_\theta \right|^2 + \left| \hat{E}_\theta \right|^2 \right|}{\left| E^{inc} \right|^2} \tag{62}$$

2.2.4 Application to Arbitrary Three-Dimensional Geometries

To demonstrate the versatility of the "SDT" to geometries which are not tractable by classical procedures, several basic shapes were examined. A prolate spheroid with minor axis ka = 1.7 and major axis kb = 3.4, was selected for comparison with the aforementioned sphere. In Figure 15, propagation of the incident magnetic field is along the major axis and the bistatic cross section is observed throughout the 360 degree sector. Considerable reduction in the monostatic cross section (in the 180 degree direction) was achieved. (Refer to Figure 14).

The truncated cone and cone-sphere geometries are of current interest since they conform to basic re-entry vehicle configurations. The bistatic cross-section of a truncated cone due to a plane wave incident on the tip is shown in Figure 16. The large back lobe is due to the sharp discontinuity at the base of the cone. By capping the base with a hemisphere to elminate the discontinuity, it is possible to suppress (by approximately 10db) the backlobe contribution as shown in Figure 17.

3.0 NORTHROP NORAIR'S "PHYSICAL OPTICS" PROCEDURE

3.1 General Formulation

As indicated above, solution of the general electromagnetic scattering and diffraction problem via Northrop Norair's Source Distribution Technique ("SDT")

is based upon the explicit determination of the current distribution induced on the surface of the scatterer by the incident wave. The scattered fields anywhere in space are in turn evaluated by integrating the current distribution over the entire surface. The unique feature of the "SDT" is its extreme simplicity and flexibility to solve arbitrary geometries. Since the scatterer is described in the Cartesian coordinate system, it can be approximated by a finite number of elemental surfaces completely independent of rotational or plane of symmetry. Another advantage to choosing this coordinate system is in the simplicity in evaluation of the scattered fields from the current distribution. Inasmuch as the three surface current components on each elemental surface are expressed in the Cartesian coordinates, simple trigonometric functions relate the currents to the scattered fields.

When the characteristic dimension of the scatterer lies in the resonance region (.1λ to 2λ) the induced current distribution is obtained by numerical solution of an integral equation. The integral equation is approximated by a finite difference technique which recasts the integral into a set of linear simultaneous equations and is solved by matrix inversion techniques.

When the characteristic dimension of the scatterer is greater than 2 λ, a fundamental limitation of the matrix inversion technique for solving the induced current distribution lies in the storage capacity and speed of the digital computer and therefore questions regarding the effectiveness of the techniques to handle these larger complex geometries naturally arise.

Indiscriminate use of storage tapes to accommodate larger and larger matrices would be seriously questioned since the rapidly increasing computer costs would deter the analytical procedures in favor of empirical techniques. Furthermore,

since greater accuracies are also associated with larger matrices and hence higher computer costs, cost-effectiveness must also be considered and properly weighed with accuracy requirements compatible with the overall system.

To this end Northrop Norair has utilized the well-established procedures of physical optics to determine the current distribution on "large" perfectly conducting scatterers. The surface of the scatterer is approximated by n elemental areas (expressed in Cartesian coordinates) and the surface current components are evaluated from the tangential component of the incident magnetic field at each subsurface.

$$\hat{J}_s = 2\hat{n} \times \hat{H}_t$$

where J_s = current density, n = subsurface normal,

H_t = tangential component of incident magnetic field .

The scattered field is given by

$$\hat{H}^{sc} = -\frac{1}{4\pi}\sum_s \left[\hat{J}_s \times \nabla \frac{e^{jkr}}{r}\right] \Delta s$$

where $k = \frac{2\pi}{\lambda}$ = wave number, r distance from any subsurface to the point of observation and the summation is carried out over the entire illuminated area.

As can be seen by the formulation above, a rigorous computation of RCS of even the simplest shape is a formidable task, restricted to analytical surfaces. The results for some of the tractable geometries are tabulated in Table 4 along with limits of applicability and proper formulation for regions of the dependent variables (wavelength, viewing angle, etc.). Generally the analyst must decompose the vehicle by experience and good judgement to allow application of catalogued shapes and sum

to approximate RCS. To overcome these restrictions, Northrop Norair utilized numerical procedures developed in part by the previous "SDT" program. The surface of the scatterer is approximated by n elemental areas (expressed in Cartesian coordinates) and the surface current components are explicitly evaluated and properly stored in the computer. The scattered fields and RCS are then determined from Kirchoff's integral. This computer program is designated "Physical-Optics" and is applicable to surfaces whose characteristic dimensions are large ($> 2\lambda$).

3.2 Numerical Results

To test the range of applicability of this procedure, the classical problem of scattering from a perfectly conducting sphere due to an incident magnetic field was examined. Comparison of the backscattering cross-section with classical results as a function of sphere circumference is shown in Figure 18. The agreement is quite good for values of ka greater than 11. In all cases the illuminated portion of the sphere was approximated by 2,520 subsurface elements. As a matter of interest, Figure 19 compares the bistatic cross-section for a sphere (ka = 10) with the classical series expansion results.

The flexibility of this "Physical Optics" technique for the solution of more complex geometries is demonstrated by examining the monostatic scattering from a large finite cylinder. The customary procedure to handle this geometry would be to approximate it by simpler geometries for which solutions are known (i.e., the ends by discs, cylindrical body by finite cylinder) and then sum the results in an appropriate manner to obtain the total cross-section of the original shape. These results are included in Figures 20 and 21 together with measured data obtained from Northrop Norair's radar reflectivity range. The discrepancies in vicinity of 45 degrees are due to edge effects which are ignored in the "Physical Optics" analysis. Edges and

surfaces discontinuities can be handled by including the "SDT" procedure with "Physical Optics" as outlined next.

4.0 "SDT-PHYSICAL OPTICS" PROCEDURES

The "Physical Optics" approximation technique fails to describe properly the currents on bodies in the transition region (upper end of resonant region and lower end of physical optics region). Northrop Norair's SDT and "Physical Optics" techniques are suitably combined to determine explicitly the current distributions over the entire surface and then sum them to obtain the scatter fields. The combination of the two programs is identified as "SDT-Physical Optics" ("SDT-P/O").

In Figure 22, let ACB be the illuminated region and ADB, the shadow region. The combination procedure simply applied the "Physical Optics" techniques to a portion of the illuminated area and then determines the current distribution in the shadow region by applying the "SDT" program, considering the coupling effects from the entire surface.

The improvement of the "SDT-Physical Optics" program over the "Physical Optics" technique for bodies in the transition region is clearly demonstrated in Figure 23. It is clear that a more accurate description of the currents in the shadow region has been achieved in the combination process resulting in more accurate description of the scattered fields.

5.0 EXPERIMENTAL APPARATUS

An image-plane technique was utilized to measure the current distribution and scattered fields. The general instrumentation followed along the lines of Kodis and Wetzel (Reference 18) who successfully applied it to two-dimensional surfaces.

A few modifications to their procedure was necessary to accommodate the three-dimensional geometries described in this study.

An image-plane was constructed of 1/16 inch aluminum sheeting and electrically bonded to form a continuous 16-foot x 24-foot ground plane. Flatness was held to 1/8 inch over the entire surface. Located in the center of the ground plane was a circular opening 15 inches in diameter. The well beneath the cut-out housed the measuring and positioning apparatus. An aluminum plate, together with the positioning device, was fitted into the hole flush with the surface and secured from below. Hemi-surfaces of various shapes investigated were fabricated and fastened to the aluminum plate (See Figure 24).

For the current distribution measurements, a magnetic probe mounted on a copper band was carried over the surface for various elevation angles. This, together with the option of rotating the circular plate in azimuth afforded the system with two degrees of freedom. Amplitude and phase meausrements for both elevation and azimuth positions were thus obtained.

Plane wave excitation was approximated by an H-plane flared horn fastened at one end of the image-plane. Since the mode of propagation over the image-plane was TM, all measurements were conducted for only vertical polarization.

Calibration of the system was performed on conducting spheres for which formal solutions are well-known and extensively tabulated. Results of these measurements are shown in Figures 13 and 14. The primary source of error was from reflecting edges of the ground plane. To minimize the edge effects, absorbing material was laid and secured along the entire periphery. (See Figure 25). Bistatic reflectivity measurements were also conducted on the image-plane utilizing an interferometer technique. In operation the bridge is initially nulled without the test specimen, then with it in place; the recorded difference is the measure of the scattering cross-section.

The image plane is also equipped with a rotator and transmitter mount to function as a ground plane reflectivity range as illustrated in Figure 26. A more complete description of the measurement apparatus and test procedures will be published in a forthcoming report.

6.0 CONCLUSIONS

The results of this study indicate that a useful and versatile technique has been developed for the solution of electromagnetic scattering from arbitrary shapes. It is capable of solving two- and three-dimensional scattering problems for which classical solutions are not available. For those simple geometries for which exact solutions are available for comparison, excellent agreement was found in all cases. For the other shapes the "SDT" solutions correlate well with the measured data.

Since the scatterer is described in the Cartesian coordinate system, it can be approximated by a finite number of elemental surfaces completely independent of rotational or plane of symmetry. Another advantage of choosing this coordinate system is the simplicity in the evaluation of the scattered fields from the current distribution. As the three surface current components on each elemental surface are expressed in the Cartesian coordinates, simple trigonometric functions relate the currents to the scattered fields in their appropriate designations.

Although developed primary for the "resonant" frequency range, the "SDT" program has been suitably combined with large body approximation procedures, "SDT-Physical Optics," handle larger geometries with greater ease and flexibility then present-day approximation procedures.

REFERENCES

1. Swan, R., "Electromagnetic Wave Reflectivity Analysis, Reduction Methods and Evaluation Techniques", Northrop Norair, NOR 62-248, December 1962.

2. Swan, R., "Radar Reflectivity Bibliography", Northrop Norair, NOR 62-139, June 1962. (This document includes a bibliography of reflectivity studies from 47 institutions and private research organizations.)

3. Sinclair, G., "Numerical Solution of Antenna and Scattering Problems", I.R.E. Transactions AP-7, December 1959.

4. Smith, A.M., "Incompressible Flow About Bodies of Arbitrary Shape", IAS National Summer Meeting, IAS Paper 62-143, June 19-22, 1962.

5. Hess, J.L., "Calculation of Potential Flow About Bodies of Revolution Having Axes Perpendicular to the Free-Stream Direction", Journal of the Aerospace Sciences, June 1962.

6. Stratton, J.A., "Electromagnetic Theory", McGraw-Hill, 1941, pages 165-169.

7. Papas, C.H., "Diffraction by Cylindrical Obstacle", Journal of Applied Physics, April 1950.

8. Maue, A.W., "Zur Formulierung eines allgemeinen Beugungs: Problems durch eine Integralgleichung, Zeitschrift fur Physik, 1949.

9. Mentzer, J.R., "Scattering and Diffaction of Radio Waves", Pergamon Press, 1955, pages 12-21.

10. Tai, C.T., "Electromagnetic Back-Scattering from Cylindrical Wires", Journal of Applied Physics, August 1952.

11. Wait, J.R., "Electromagnetic Radiation from Cylindrical Structure", Pergamon Press, 1959.

12. Tilston, W.V., "An Integral Equation Method for the Solution of Wave Equation in Certain Boundary Value Problems", McGill Symposium in Microwave Optics, Part II, April 1959.

13. Weston, V.H., "The Effect of a Discontinuity in Curvature in High Frequency Scattering", I.R.E. Transactions AP-10, November 1962.

14. Franz, W. and Depperman, K., "The Creeping Wave in the Theory of Diffraction," McGill Symposium on Microwave Optics, Part II, April 1959.

15. King, R., and Wu, T.T., "The Reflections of Electromagnetic Waves from Surfaces of Complex Shapes", Part II Theoretical Studies. Cruft Laboratory, Harvard University Scientific Report 13, December 1957.

16. Fock, V., "The Distribution of Currents Induced by a Plane Wave on the Surface of a Conductor", Journal of Applied Physics. (U.S.S.R.) 10, 130 (1946).

17. Wetzel, L., "High Frequency Current Distributions on Conducting Obstacles", Scientific Report No. 10, Cruft Laboratory, Harvard University, May 1957.

18. Wetzel, L., and Brick, B.D., "An Experimental Investigation on the Fock Approximation for Conducting Cylinders", I.R.E. Transactions AP-8, November 960.

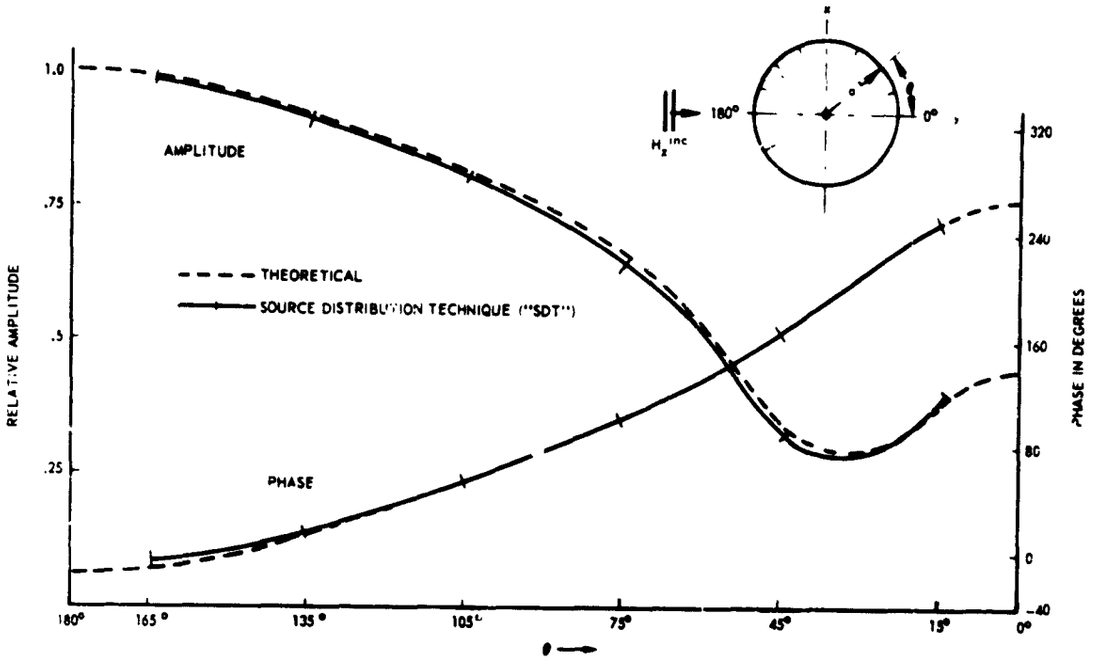

FIGURE 1 CURRENT DISTRIBUTION ON CIRCULAR CYLINDER, H_z^{inc} (VERT. POL.) (ka = 1.6)

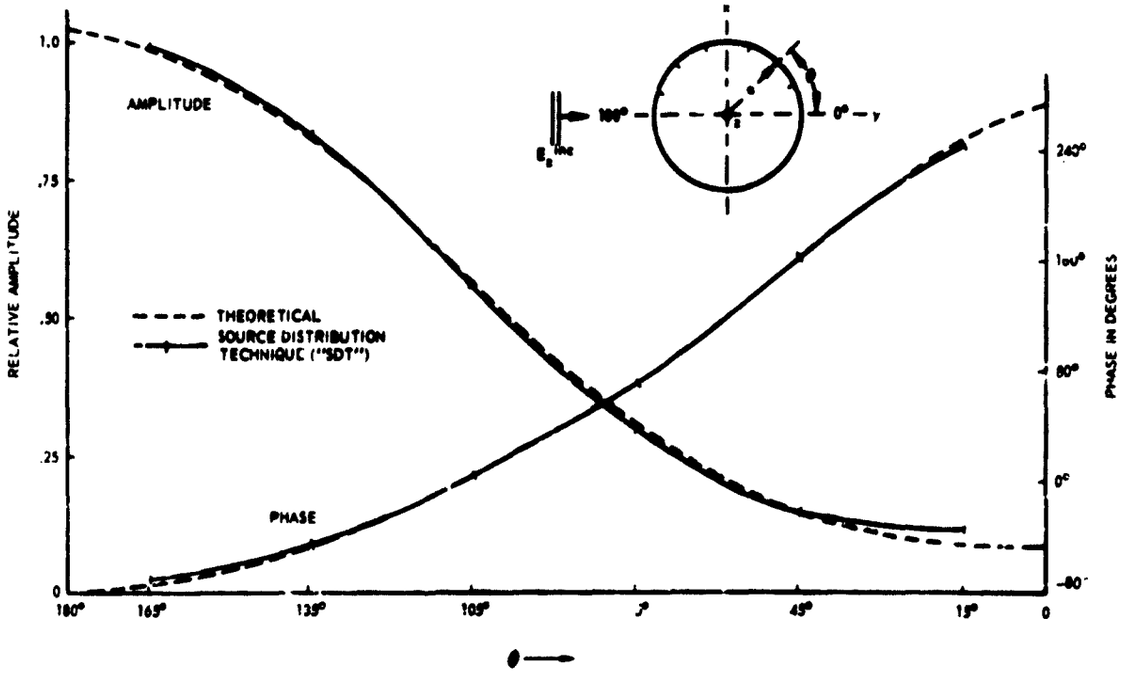

FIGURE 2 CURRENT DISTRIBUTION ON CIRCULAR CYLINDER, E_z^{inc} (HOR. POL.) (ka = 1.6)

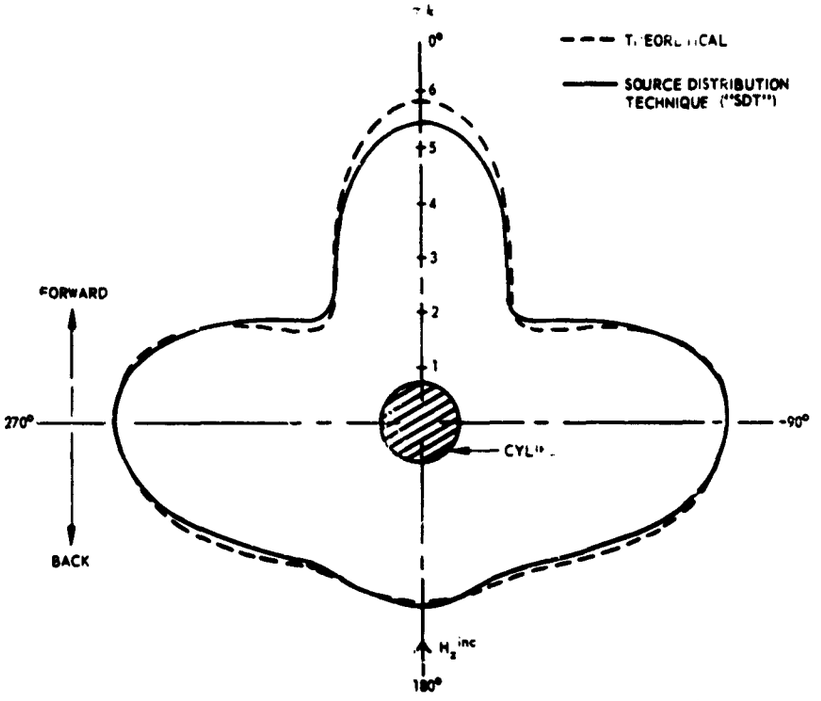

FIGURE 3 SCATTERING CROSS-SECTION OF CIRCULAR CYLINDER, H_z^{inc} (VERT. POL.) (ka = 1.6)

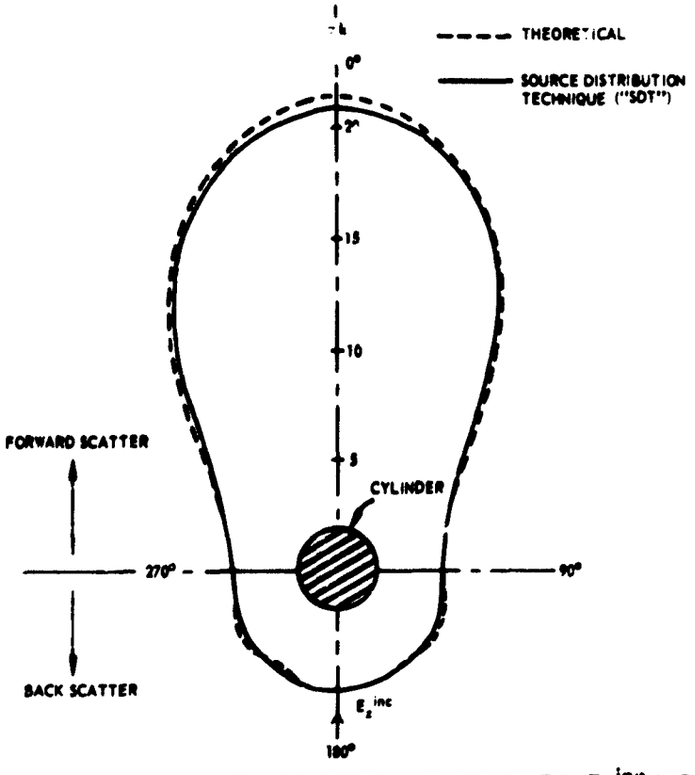

FIGURE 4 SCATTERING CROSS-SECTION OF CIRCULAR CYLINDER, E_z^{inc} (HOR. POL.) (ka = 1.6)

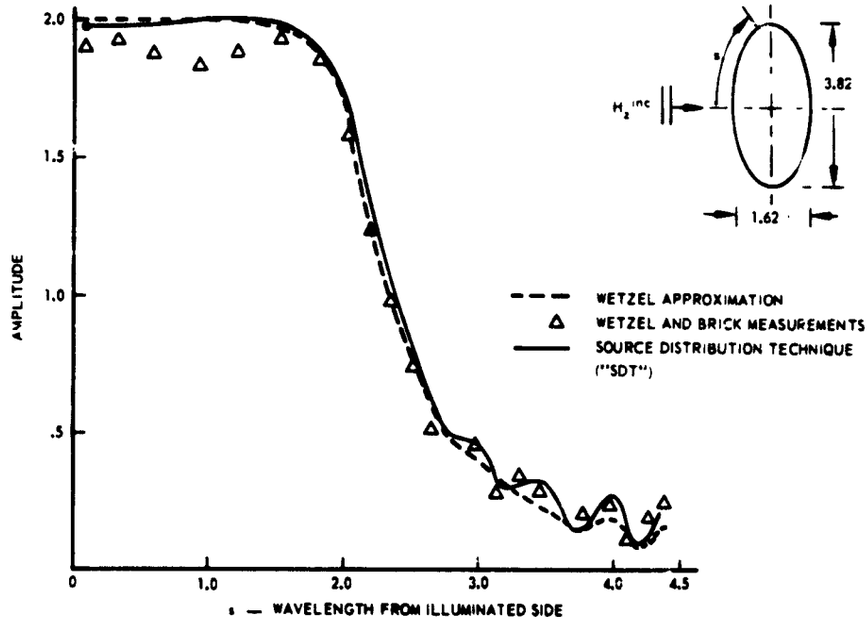

FIGURE 5 CURRENT AMPLITUDE DISTRIBUTION ON ELLIPTIC CYLINDER, H_z^{inc} (VERT. POL.)

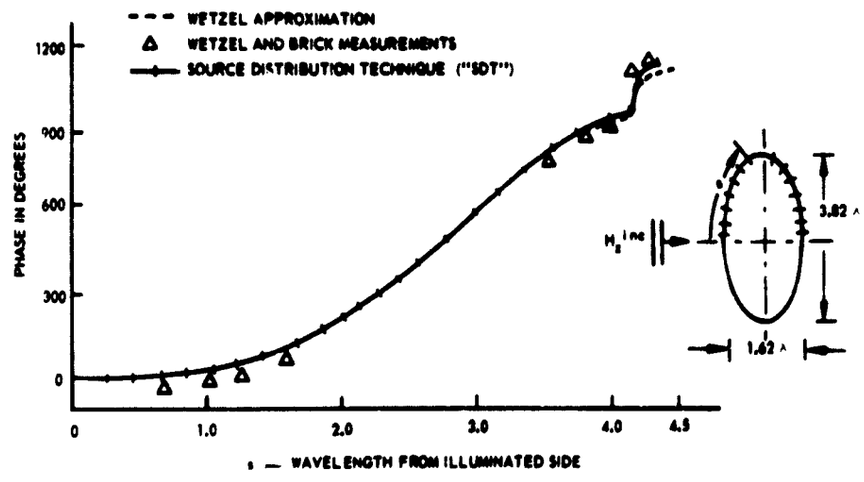

FIGURE 6 CURRENT PHASE DISTRIBUTION ON ELLIPTIC CYLINDER, H_z^{inc} (VERT. POL.)

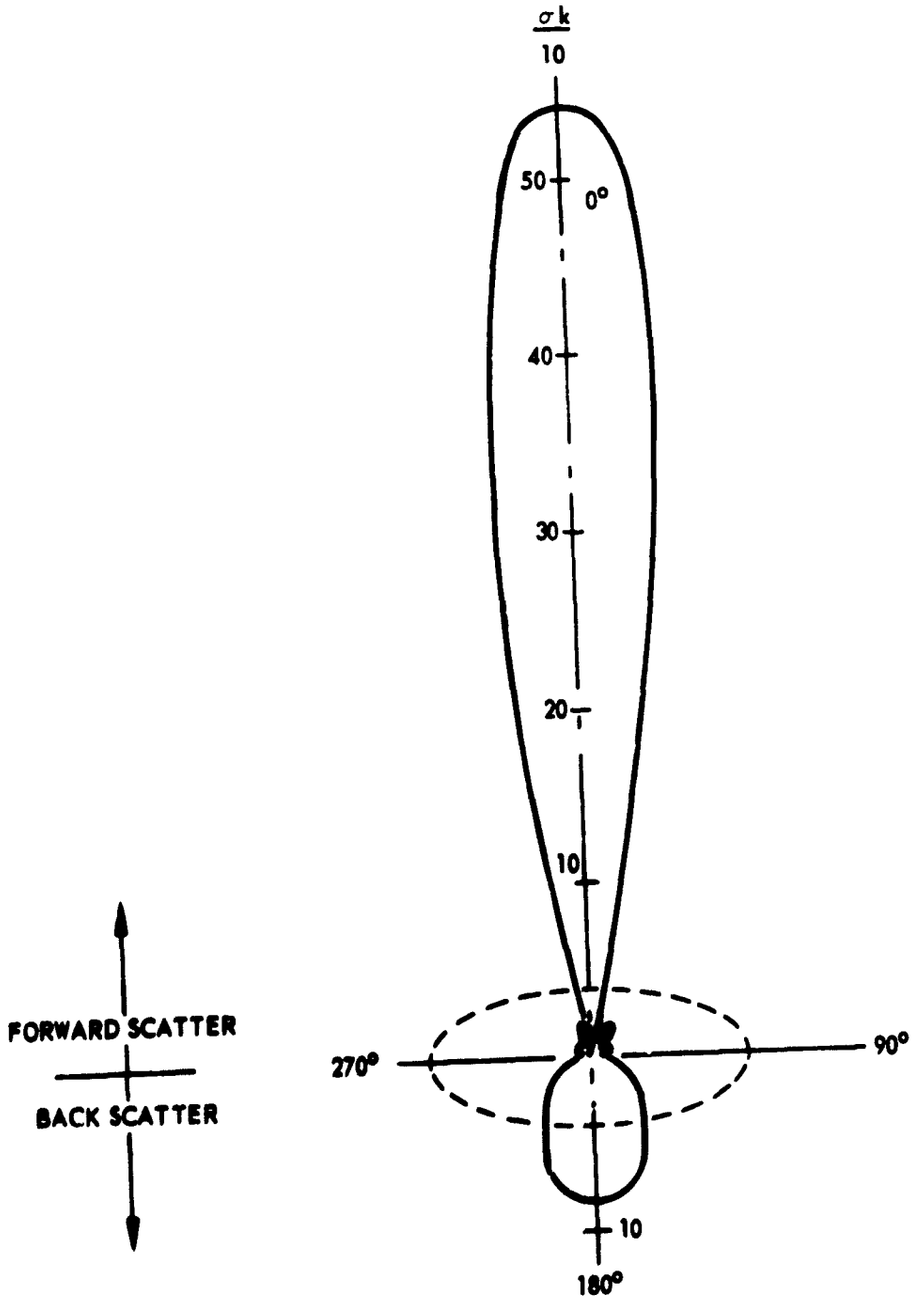

FIGURE 7 SCATTERING CROSS-SECTION OF ELLIPTIC CYLINDER, H_z^{inc} (VERT. POL.)

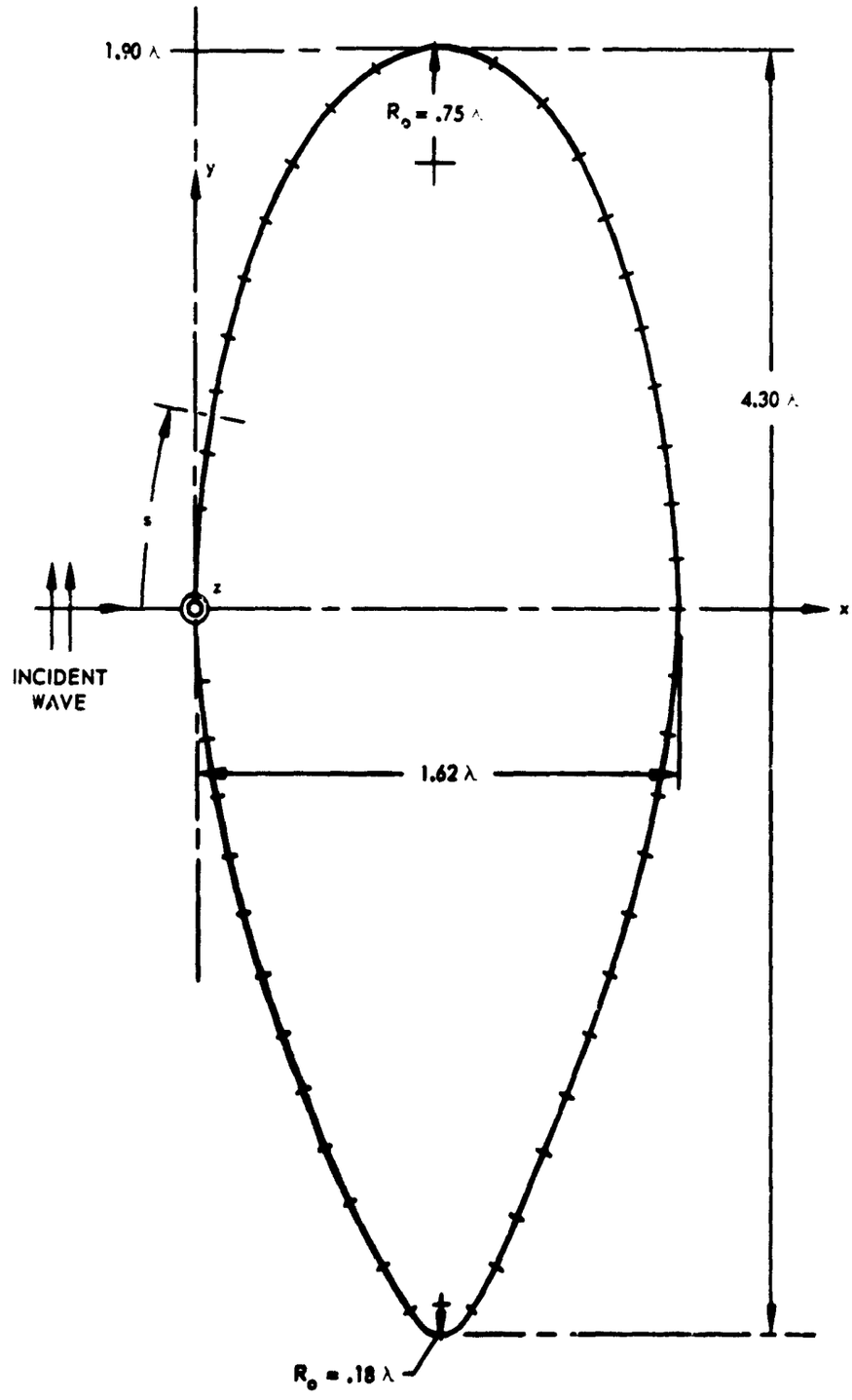

FIGURE 8 AIRFOIL SECTION NO. 1

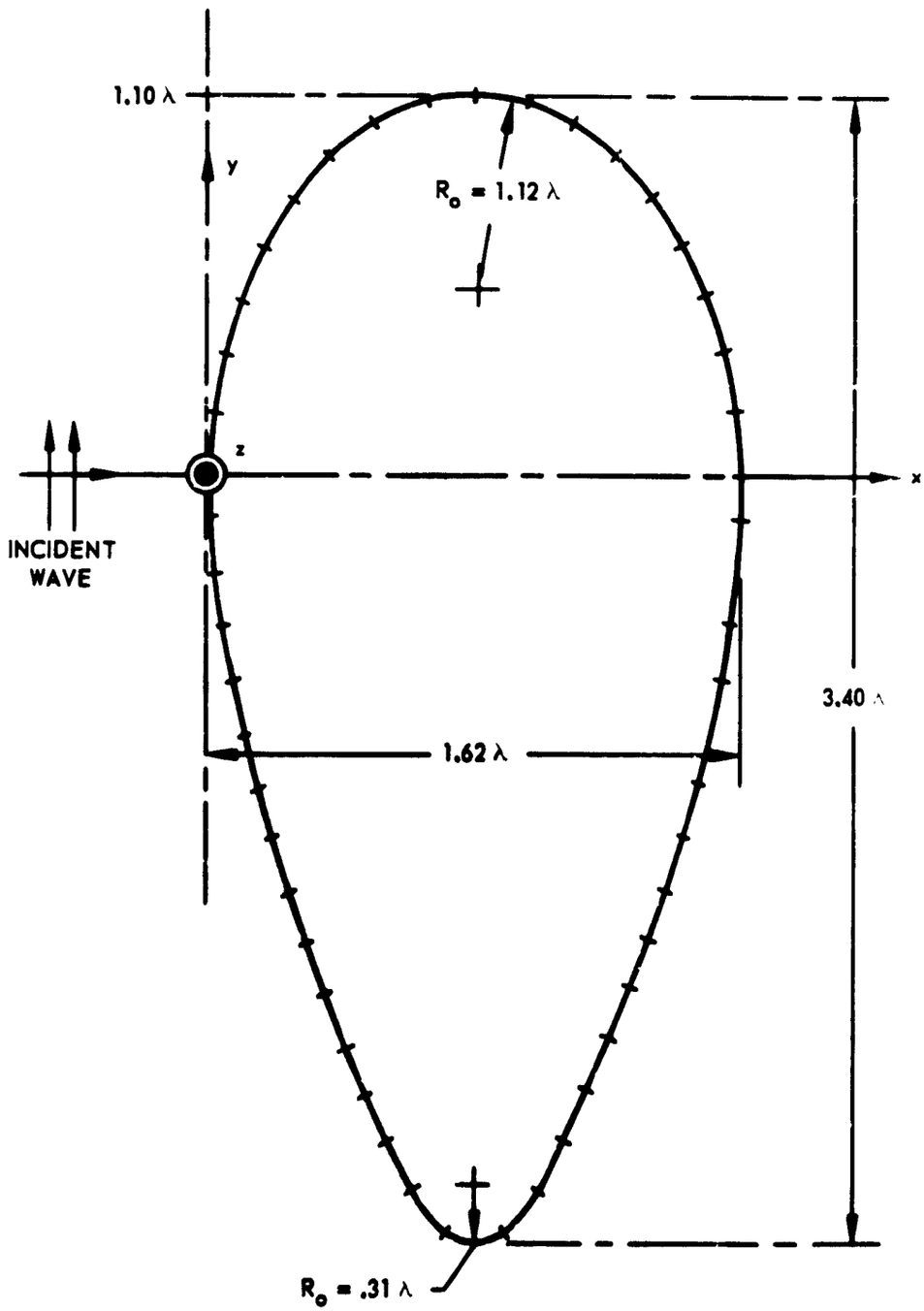

FIGURE 9 AIRFOIL SECTION NO. 2

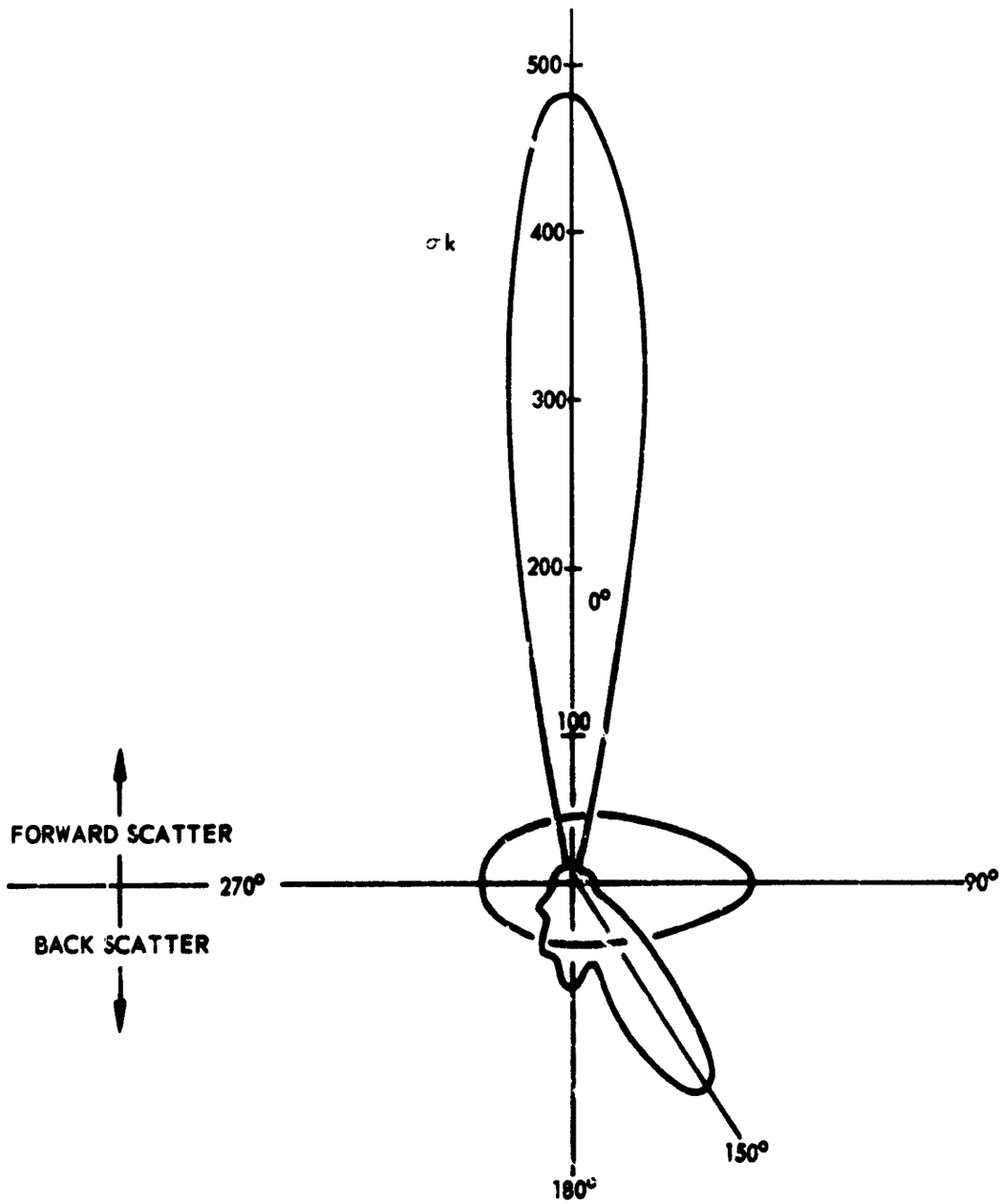

FIGURE 11 SCATTERING CROSS-SECTION OF AIRFOIL NO. 2, H_z^{inc} (VERT. POL.)

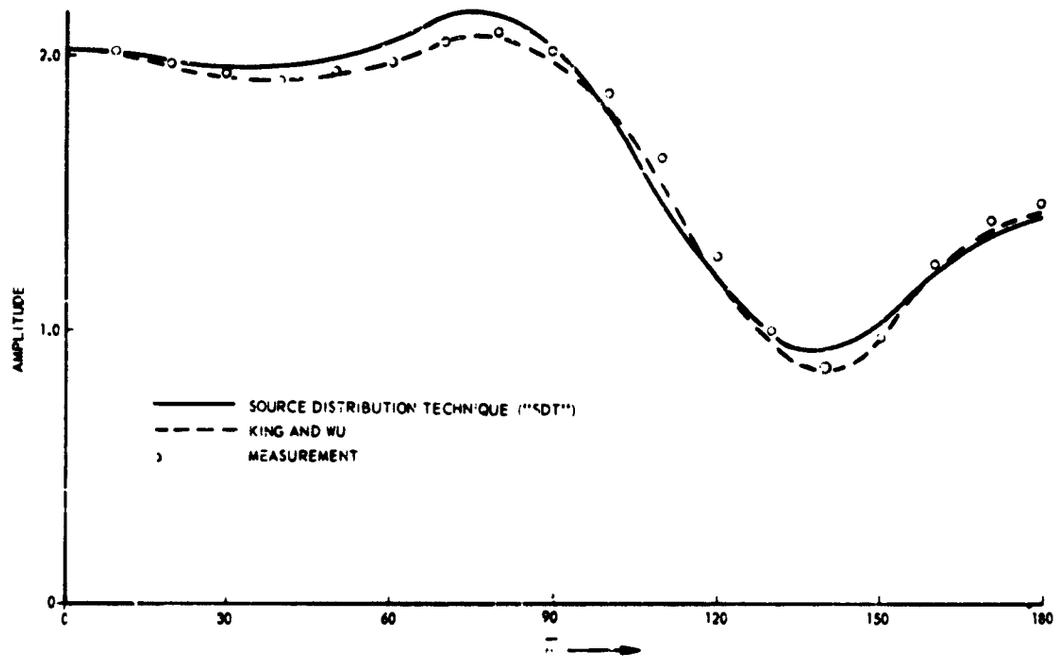

FIGURE 12 CURRENT DISTRIBUTION ON SPHERE $F_\theta(\theta)$ COMPONENT, (ka = 1.7)

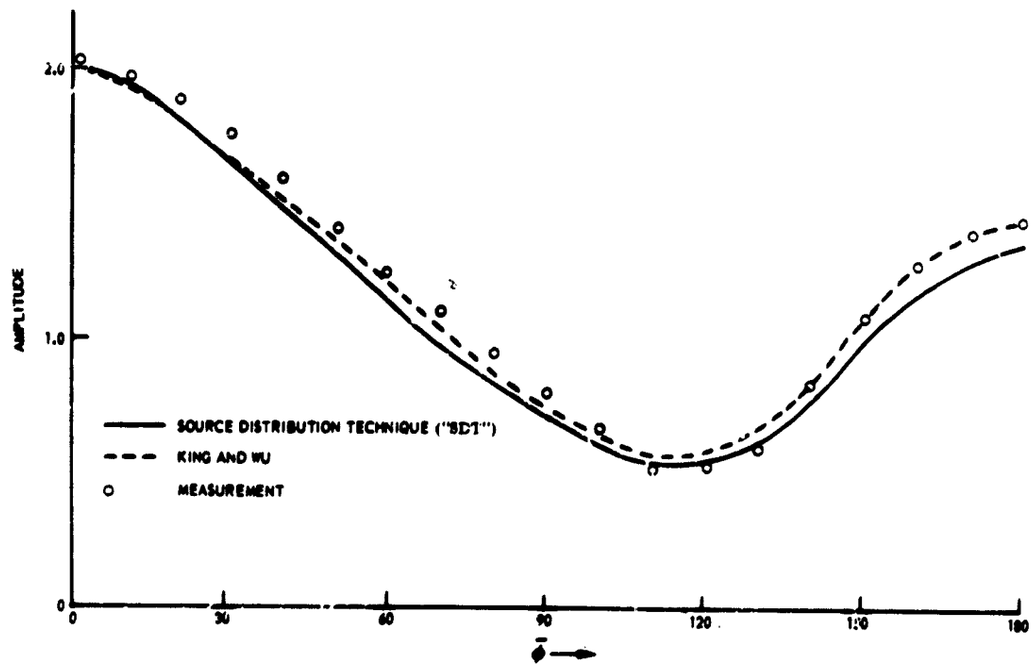

FIGURE 13 CURRENT DISTRIBUTION ON SPHERE $F_\theta(\phi)$ COMPONENT, (ka = 1.7)

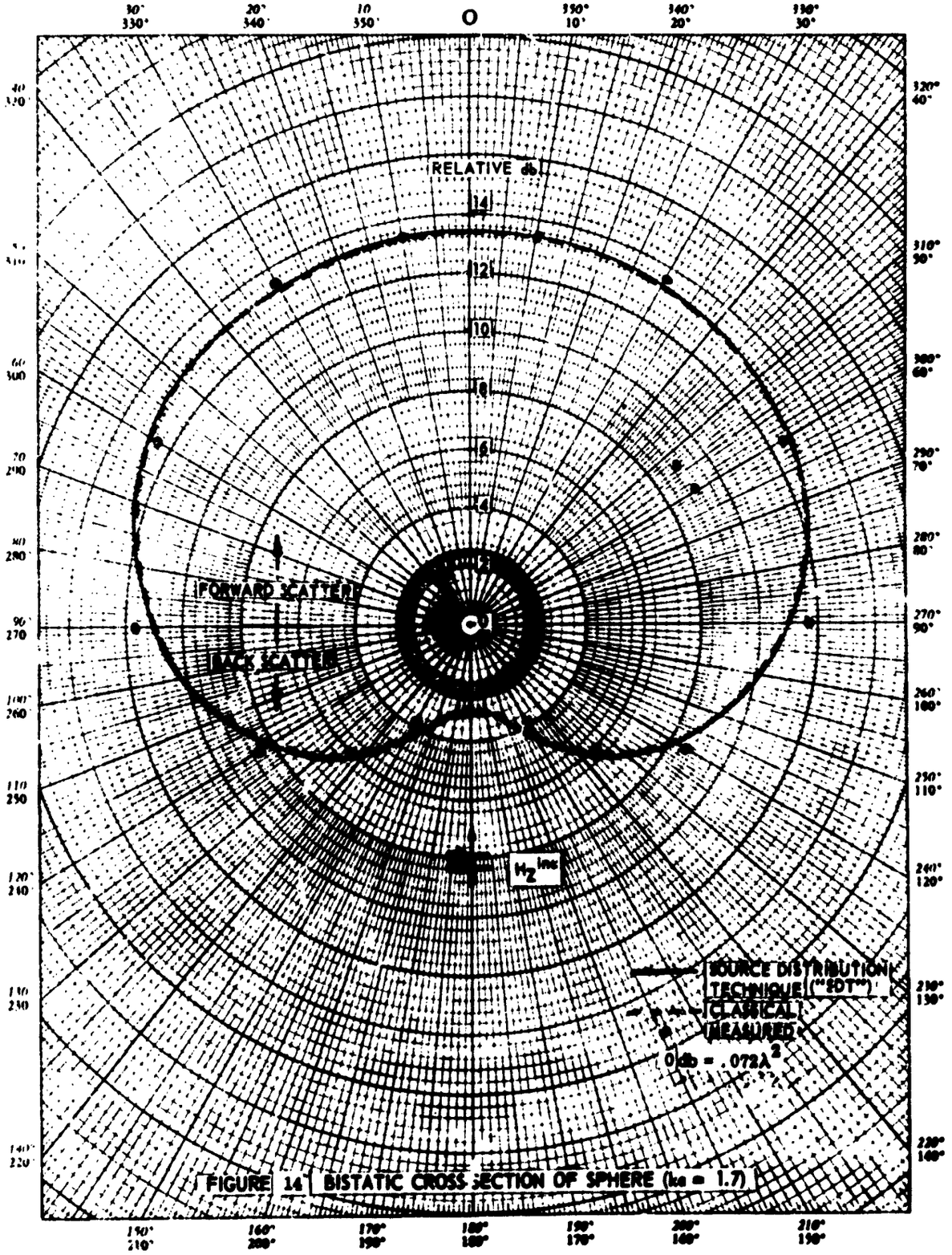

FIGURE 14 BISTATIC CROSS SECTION OF SPHERE (ka = 1.7)

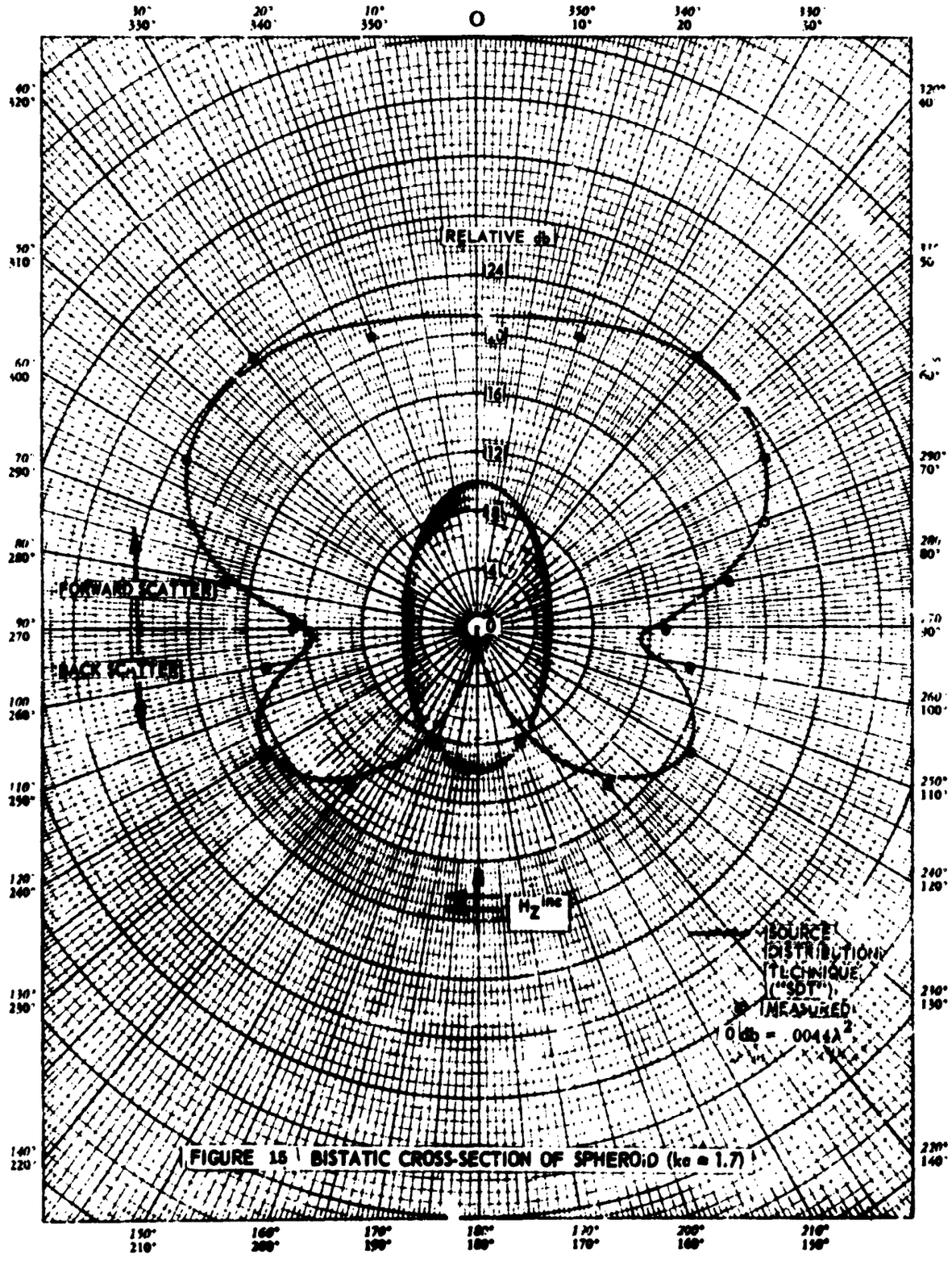

FIGURE 15 BISTATIC CROSS-SECTION OF SPHEROID (ka = 1.7)

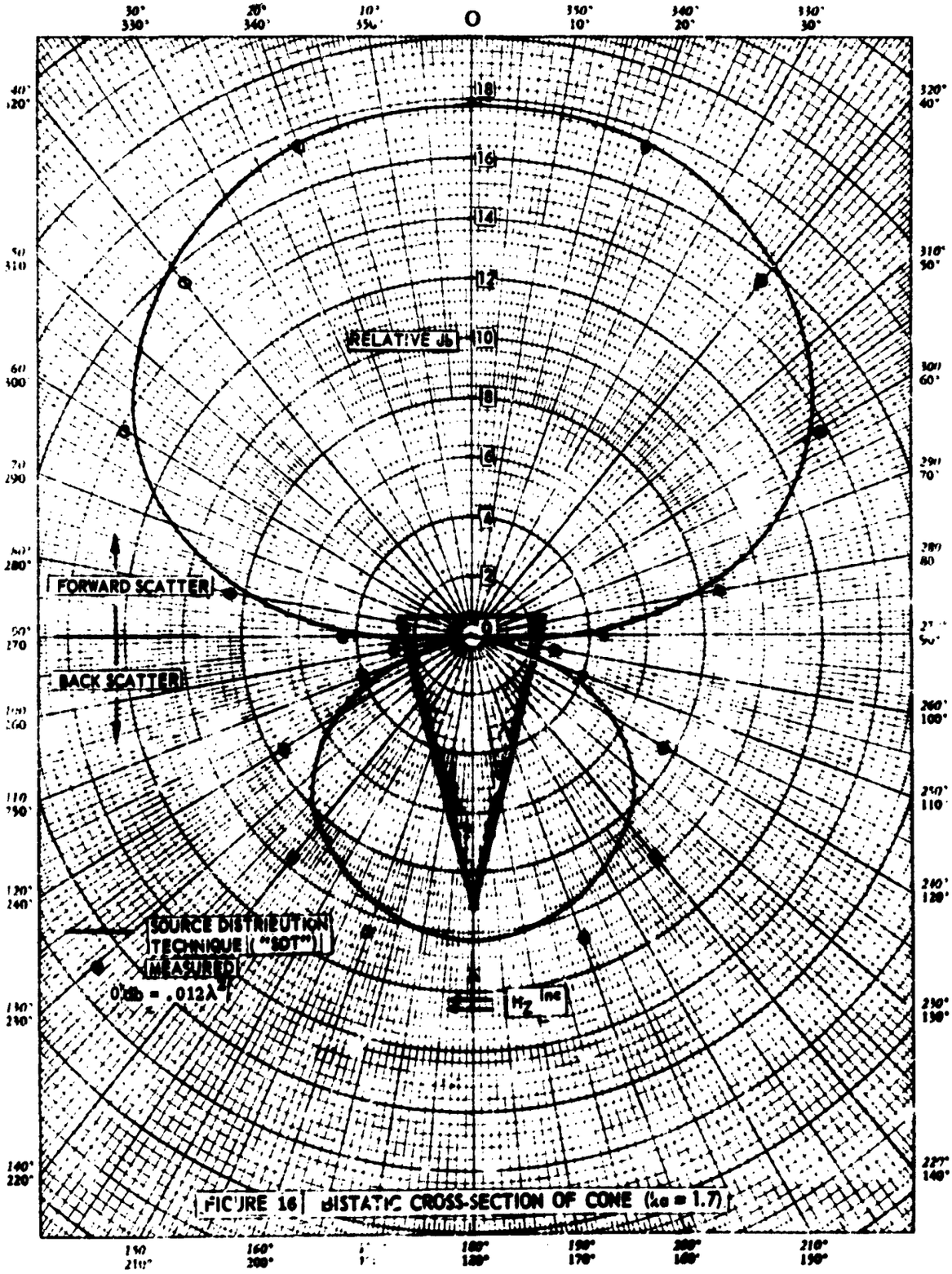

FIGURE 16 BISTATIC CROSS-SECTION OF CONE ($ka = 1.7$)

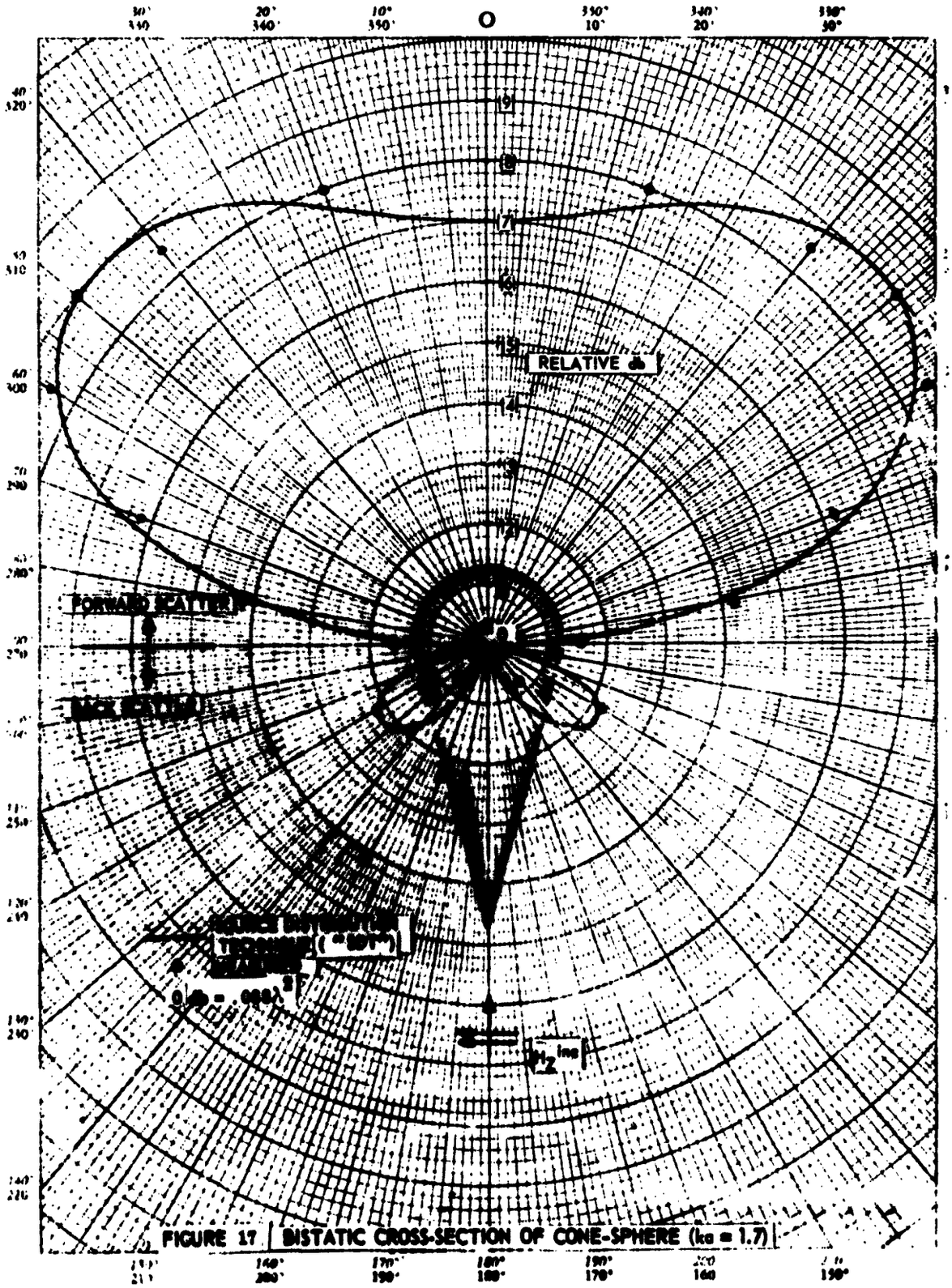

FIGURE 17 | BISTATIC CROSS-SECTION OF CONE-SPHERE (ka = 1.7)

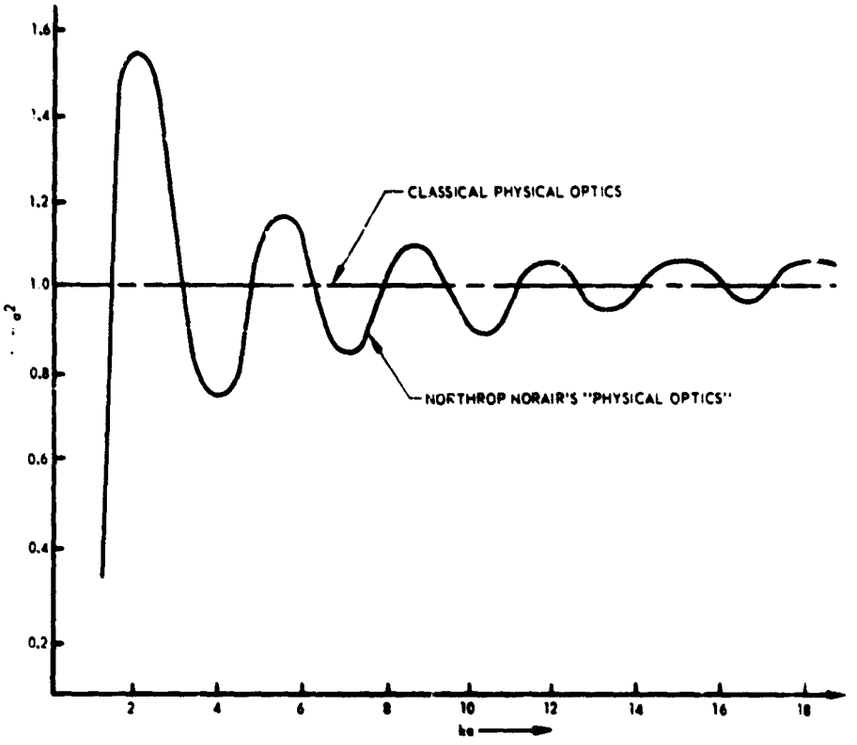

FIGURE 18 BACKSCATTERING CROSS-SECTION OF PERFECTLY CONDUCTING SPHERE

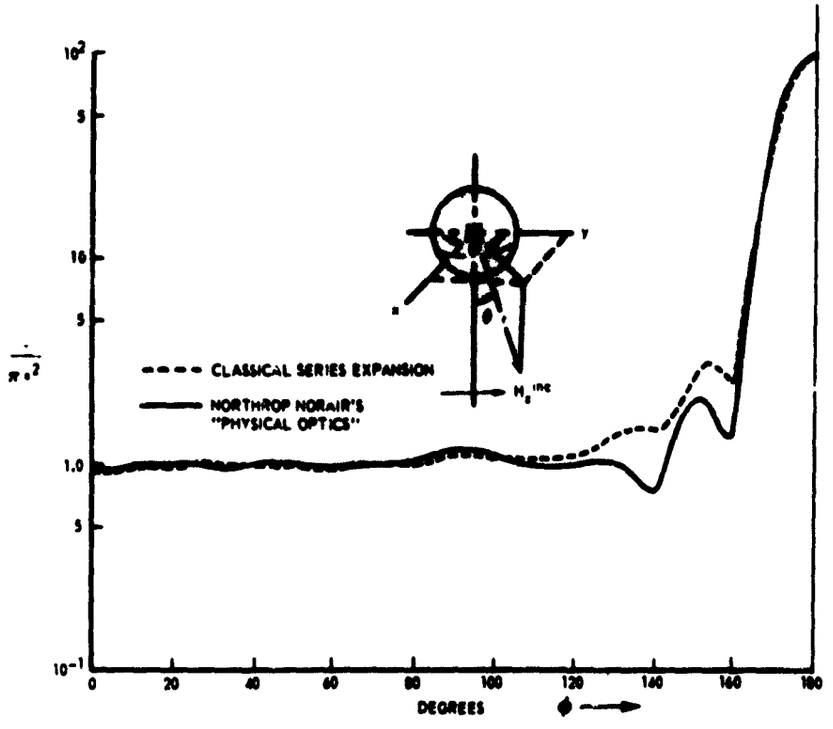

FIGURE 19 BISTATIC CROSS-SECTION FOR PERFECTLY CONDUCTING SPHERE (ka = 10) H-PLANE

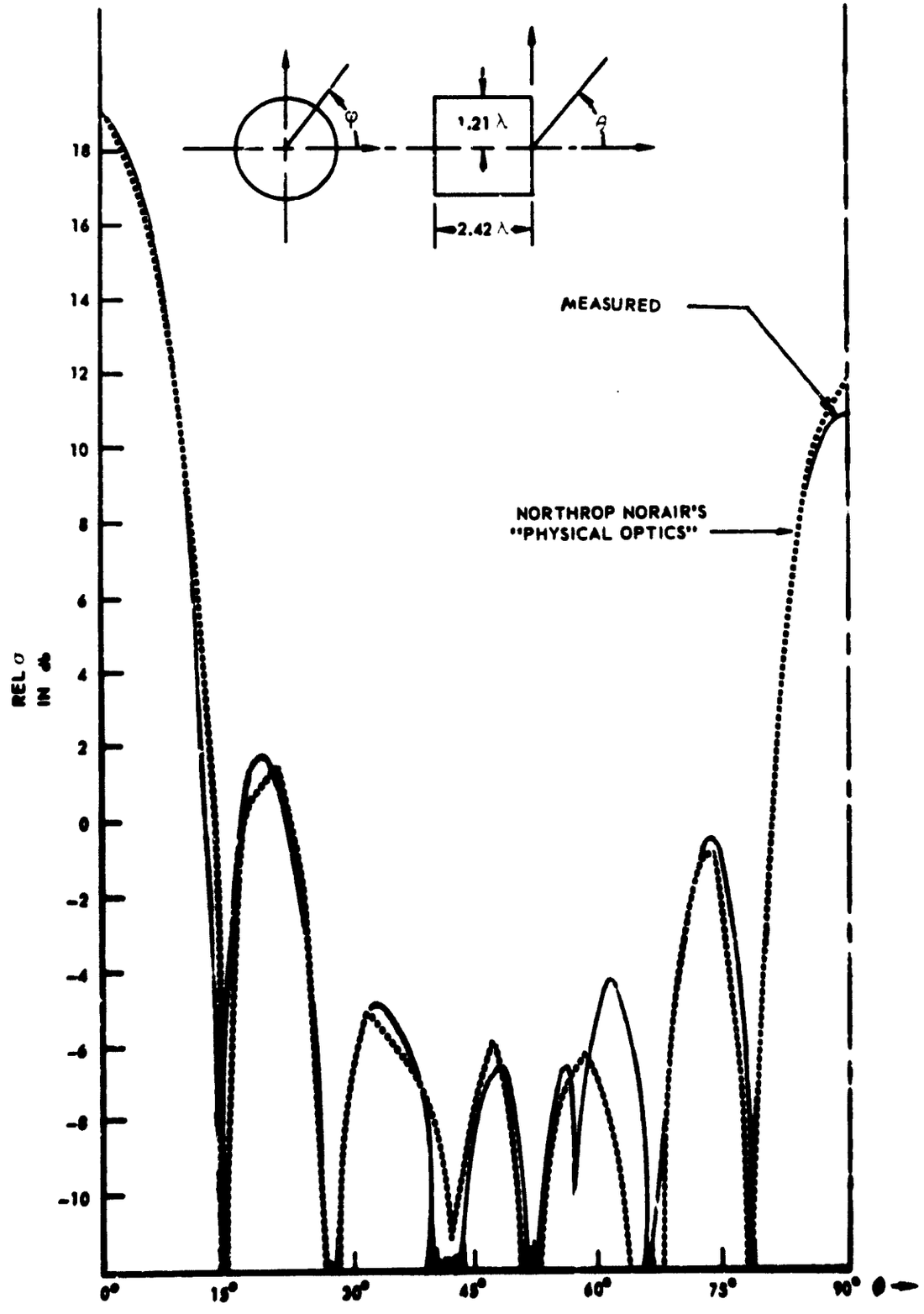

FIGURE 20 MONOSTATIC CROSS-SECTION OF CIRCULAR CYLINDER
(R = 1.21 λ, L = 2.42 λ)

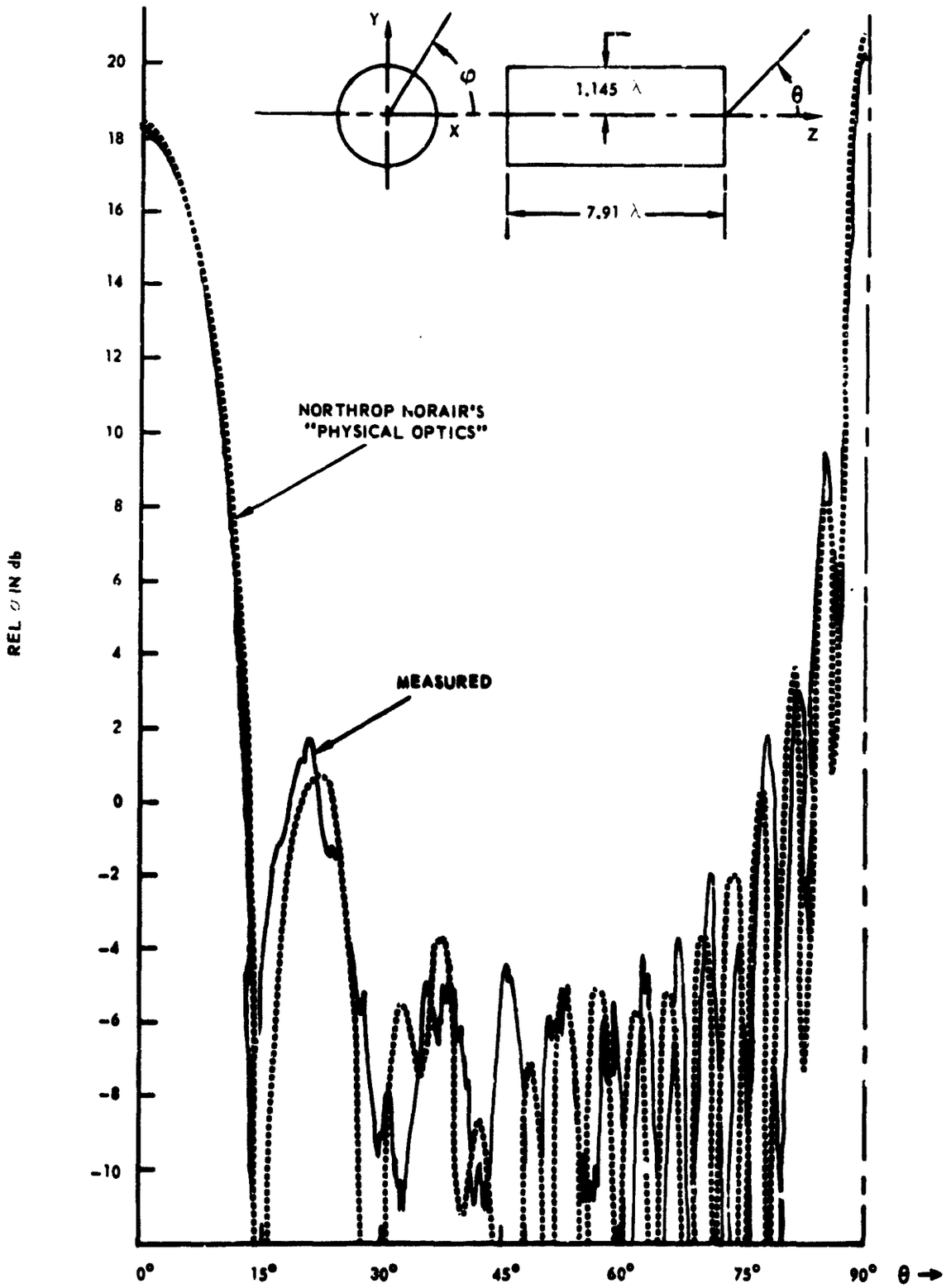

FIGURE 21 MONOSTATIC CROSS-SECTION OF CIRCULAR CYLINDER
(R = 1.145 λ, L = 7.91 λ)

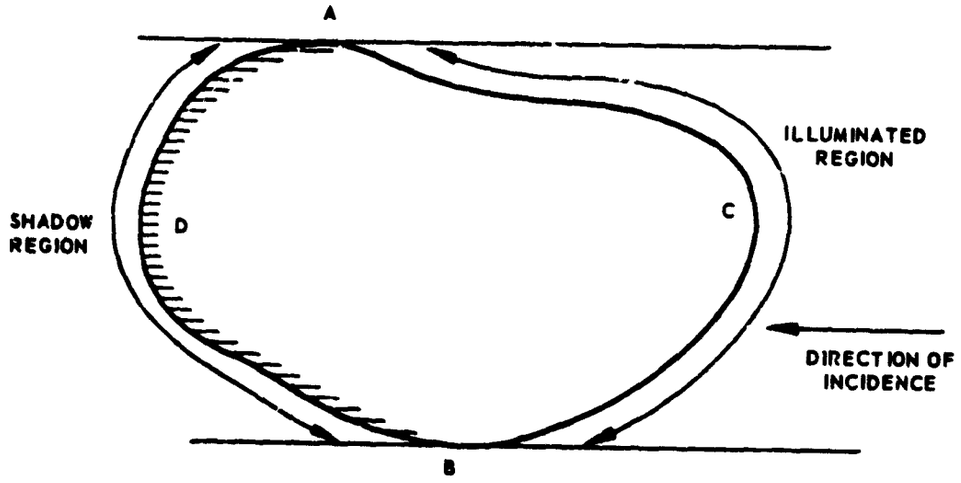

FIGURE 22. APPLICATION OF "SDT-P/O" TECHNIQUES ON BODIES IN TRANSITION REGI

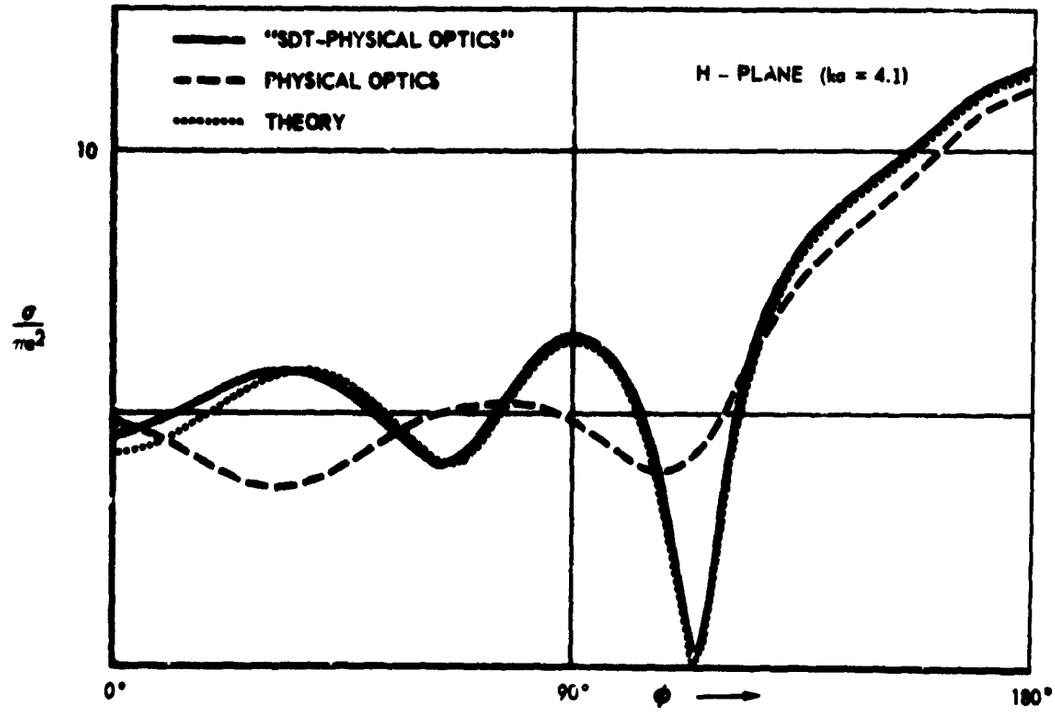

FIGURE 23. "SDT - PHYSICAL OPTICS" BISTATIC CROSS SECTION OF SPHERE (ka = 4

FIGURE 24. HEMI-SURFACE MOUNTED ON IMAGE-PLANE

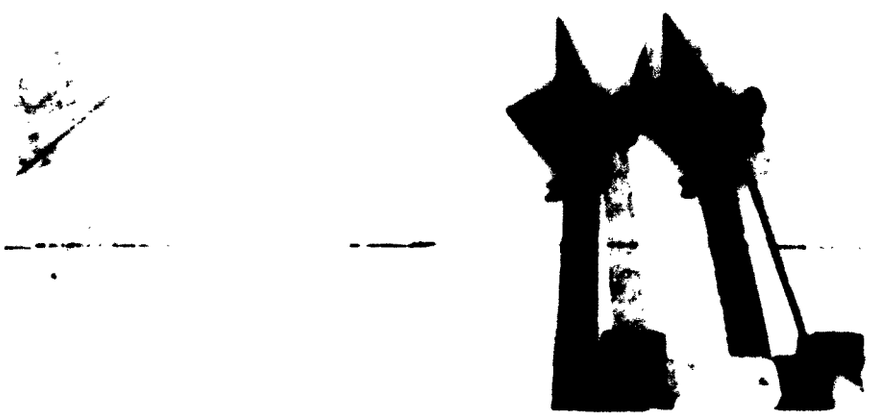

FIGURE 25. IMAGE-PLANE WITH ABSORBING MATERIAL

FIGURE 26. GROUND PLANE REFLECTIVITY RANGE

TABLE 1 RADAR CROSS SECTION (σ) OF SOME SIMPLE SHAPES

SHAPE	PERTINENT DIMENSIONS (AND POLARIZATION)*	VIEWING ORIENTATION (AND BODY WAVELENGTH CONDITIONS)**	RADAR CROSS SECTION σ
Sphere	Radius = a Wavelength = λ $k = \frac{2\pi}{\lambda}$	(ka 30) (ka = 1) (ka .05)	πa^2 $3.65\pi a^2$ $9(ka)^4 \pi a^2$
Doubly Curved Surface	Radii = a_1 and a_2	Normal to Surface	$\pi a_1 a_2$
Ellipsoid, General Ellipsoid of Revolution	Semi-Axes a, b, c. Semi-Axes a = b, c	ϕ to a-Axis θ to c-Axis θ to c-Axis	$\frac{\pi a^2 b^2 c^2}{(a^2 \sin^2\theta\cos^2\phi + b^2 \sin^2\theta \sin^2\phi + c^2\cos^2\theta)^2}$ $\frac{\pi b^4 c^2}{(b^2\sin^2\theta + c^2\cos^2\theta)^2}$
Ogive of Revolution	Diameter d Length = ℓ	Normal to Axis	$\frac{\pi}{8}(\ell^2 + d^2)$
Flat Circular Plate	Radius = a $u = \frac{4\pi a \sin\phi}{\lambda}$ (J_1 = 1st Order Bessel Function)	At Angle ϕ to Normal	$\frac{4\pi^3 a^4}{\lambda^2}\left[2\frac{J_1(u)}{u}\right]^2 \cos^2\phi$
Flat Plate	Area = S	Normally Peaks at Small ϕ Excluding Peak at Normal Incidence	$4\pi(S/\lambda)^2$ $\frac{4\pi A^2}{(2\pi\phi)^4}$
Plane or Thin Wedge	Edge Length = ℓ (Polarization to Edge)	Edge On	$\frac{\ell^2}{2\pi}$
Cylinder	Radius = a Length = ℓ $N = \frac{2\pi\ell\sin\phi}{\lambda}$	At Angle ϕ from Normal to Axis Peak at Small ϕ Excluding Peak at Normal Incidence	$\frac{2\pi a\ell^2}{\lambda}\left(\frac{\sin N}{N}\right)^2\cos\phi$ $\frac{a\lambda}{2\pi\phi^2}$
Elliptical Cylinder	Length = ℓ Semi-Axes = a, b	Normal to Axis of Cylinder and at Angle ϕ to a-Axis	$\frac{2\pi\ell^2 a^2 b^2}{\lambda(a^2\cos^2\phi + b^2\sin^2\phi)^{3/2}}$
Infinite Cone (Conical Tip)	Half Angle = θ	Axially	$\lambda^2\tan^4\theta\ 16\pi$
Cone	(Height = h Half Angle = θ (Small θ) Base Radius = a)	Axially Nose-On	$\pi a^2\tan^2\theta = \pi h^2\tan^4\theta$
		Normal to Conic Surface	$\frac{8\pi a^3}{9\lambda\sin^2\theta\cos\theta} = \frac{8\pi h^3\sin\theta}{9\lambda\cos^4\theta}$
	(θ = from Axis)	$0 < \theta < \theta$	$\frac{\lambda h\tan\theta}{8\pi\lvert\sin\theta\rvert}\left[\tan^2(\theta+\theta) + \tan^2(\theta-\theta)\right]$
		$\theta < \theta < \frac{\pi}{2} - \theta$	$\frac{\lambda h\tan\theta}{8\pi\lvert\sin\theta\rvert}\tan^2(\theta+\theta)$
		$\frac{\pi}{2} < \theta < \pi - \theta$	$\frac{\lambda h\tan\theta}{8\pi\lvert\sin\theta\rvert}\left[\frac{1}{\sin^2\theta(-\cos\theta + \tan\theta\lvert\sin\theta\rvert)^2} \cdot \frac{1}{\sin^2\theta\cos^2\theta}\right]$
Frustum of Cone	Half Angle = θ Smaller Radius = a_1 Larger Radius = a_2	Normal to Conic Surface	$\frac{8\pi\left(a_2^{3/2} - a_1^{3/2}\right)^2}{9\lambda\sin^2\theta\cos\theta}$
Corner Reflector	Each 90° Edge = a	At Maximum θ	$\frac{4\pi a^4}{3\lambda^2}$

*When not specified, polarization is not critical
**When not specified, wavelength -- body dimensions

TABLE 1 RADAR CROSS SECTION (σ) OF SOME SIMPLE SHAPES (CONTINUED)

SHAPE	PERTINENT DIMENSIONS (AND POLARIZATION)*	VIEWING ORIENTATION (AND BODY WAVELENGTH CONDITIONS)**	RADAR CROSS SECTION σ
Paraboloid	$x^2 + y^2 = 4pz$	At angle θ from Axis	$4\pi p^2 \sec^4 \theta$
Wire	Euler's constant = γ = 1.781 Radius of wire = a Length of wire = L Polarization at angle θ from parallel to axis	At angle θ to Axis	$\pi L^2 \sin^2 \theta \left[\frac{\sin\left(\frac{2\pi L}{\lambda} \cos\theta\right)}{\frac{2\pi L}{\lambda} \cos\theta} \right]^2 \Big/ \left(\frac{\pi}{2}\right)^2 \left(\log \frac{\lambda}{\gamma\pi a \sin\theta}\right)^2 \cos^4 \theta$
Flat Rectangular Plate	Dimension a x b Angle ϕ measured from coordinate a	At angle θ from Normal	$\frac{4\pi (ab)^2}{\lambda^2} \left[\frac{\sin (ka \sin\theta \cos\phi)}{ka \sin\theta \cos\phi} \frac{\sin (kb \sin\theta \sin\phi)}{kb \sin\theta \sin\phi} \right]^2 \cos^2 \theta$
Truncated Ogive	Ogive angle σ at nose. Ogive angle σ' at a' Minor radius of ogive a Major radius of ogive a Ogive radius R	At angle θ from axis of ogive $0 < \theta < \sigma'$ and $\theta < \frac{\pi}{2} - \sigma$ $\sigma' < \theta < \left(\frac{\pi}{2} - \sigma\right)$ $\theta > \frac{\pi}{2} - \sigma$	$\frac{\lambda a' \tan^2 (\theta - \sigma')}{8\pi \sin\theta} + \frac{\lambda a' \tan^2 (\theta + \sigma')}{8\pi \sin\theta}$ $\frac{\lambda a' \tan^2 (\theta + \sigma')}{8\pi \sin\theta}$ $= \pi \left(1 - \frac{R - a}{R \sin\theta}\right)^2$

*When not specified, polarization is not critical
**When not specified, wavelength << body dimensions